

Explainable Anomaly Detection in Images and Videos: A Survey

Yizhou Wang^{1*†}, Dongliang Guo^{2*†}, Sheng Li², Octavia Camps¹, Yun Fu^{1,3}

¹Department of Electrical and Computer Engineering, Northeastern University, 100 Forsyth St, Boston, 02115, MA, USA.

²School of Data Science, University of Virginia, 400 Brandon Ave, Charlottesville, 22903, VA, USA.

³Khoury College of Computer Science, Northeastern University, 440 Huntington Ave, Boston, 02115, MA, USA.

*Corresponding author(s). E-mail(s): wyzjack990122@gmail.com;
dongliang.guo@virginia.edu;

Contributing authors: vga8uf@virginia.edu; camps@ece.northeastern.edu;
yunfu@ece.neu.edu;

[†]These authors contributed equally to this work.

Abstract

Anomaly detection and localization of visual data, including images and videos, are of great significance in both machine learning academia and applied real-world scenarios. Despite the rapid development of visual anomaly detection techniques in recent years, the interpretations of these black-box models and reasonable explanations of why anomalies can be distinguished out are scarce. This paper provides the first survey concentrated on explainable visual anomaly detection methods. We first introduce the basic background of image-level and video-level anomaly detection. Then, as the main content of this survey, a comprehensive and exhaustive literature review of explainable anomaly detection methods for both images and videos is presented. Next, we analyze why some explainable anomaly detection methods can be applied to both images and videos and why others can be only applied to one modality. Additionally, we provide summaries of current 2D visual anomaly detection datasets and evaluation metrics. Finally, we discuss several promising future directions and open problems to explore the explainability of 2D visual anomaly detection. The related resource collection is given at <https://github.com/wyzjack/Awesome-XAD>.

Keywords: Anomaly Detection, Explainable Machine Learning, Image Processing, Video Processing

1 Introduction

Anomaly detection plays a crucial role in society. Nowadays, with the development technique of computer vision, many researchers try to address 2D anomaly detection tasks, including image

anomaly detection (Reiss et al, 2021; Pang et al, 2021; Roth et al, 2022; Cohen and Avidan, 2022) and video anomaly detection (Georgescu et al, 2021a; Liu et al, 2021; Chen et al, 2022; Liu et al, 2018; Yu et al, 2020; Wang et al, 2022a; Georgescu

et al, 2021b). 2D anomaly detection aims to identify unusual or abnormal patterns in visual data, such as images and videos. It is used in various applications, such as surveillance, security, medical imaging, and industrial inspection. The basic idea behind 2D anomaly detection is to train a model to recognize normal patterns in a set of training data, and then use that model to identify instances where new, unseen data deviates from those normal patterns. Considering the nature of the data, most of the statistic methods, like isolation forest and KNN, that work well on tabular data cannot directly apply to image data. Deep learning-based methods are extensively employed in 2D anomaly detection. For example, Autoencoders and Variational Autoencoders (VAEs) are common architectures used in 2D anomaly detection. Autoencoders are neural networks that are trained to reconstruct their input by learning a compact representation of the data. VAEs are a probabilistic extension of autoencoders that learn a generative model of the data. Through training these models on a dataset of normal images, it can be used to identify images that deviate significantly from the normal patterns.

Although existing work has proved the potential of deep learning models to identify anomalies in visual data, the explainability of those works is limited. Explainability is defined as the ability to explain or provide meaning to humans in understandable terms. As for the 2D anomaly detection task, an explainable model should give appropriate and faithful reasons for making such decisions. In fact, model explainability represents one of the main issues concerning the adoption of data-driven algorithms in industrial environments (Langone et al, 2020; Li et al, 2023b). More importantly, providing explanations for AI systems is now both an ethical and a regulatory requirement, especially in fields where human safety is a concern. For example, in the biomedical image anomaly detection task, a deep learning model can give a precise prediction for X-ray images with respect to disease, but without any explanation. However, it is very risky to fully trust it. In many other cases, our goal is not only to detect anomalies but also to localize them and explain them so that we can troubleshoot those anomalies and fix them eventually. Thus, explainable 2D anomaly detection is necessary and important for a wide variety of human activities.

To tackle this issue, some methods have been proposed in recent years. For different tasks and user orientations, the explanation proposals are largely different, which causes the appearance of numerous explainable methods. For example, in the surveillance video anomaly detection task, Szymanowicz et al (2022) uses an autoencoder-based method to detect anomalies, and the prediction error is constructed as a saliency map with which off-the-shelf object detection and action recognition model are applied to explain anomalies post hoc. In this survey, we focus on existing methods related to 2D anomaly detection tasks. In particular, we classify them into two types: image anomaly detection and video anomaly detection.

To the best of our knowledge, anomaly detection has been widely studied, and there exists a lot of surveys (Mohammadi et al, 2021; Ramachandra et al, 2020; Jiang et al, 2022; Cao et al, 2024) about them. In contrast, there are a limited number of existing surveys on the topic of explainable anomaly detection (Li et al, 2023b). Moreover, those existing surveys try to review all explanation methods with respect to all kinds of data types, which provide a good overview but lack insightful direction in 2D anomaly detection. In addition, there is no such survey in the explainable 2D anomaly detection area, and thus it is necessary to characterize the increasingly rich set of explainable 2D anomaly detection techniques available in the literature. In order to tackle this challenge, we conduct a comprehensive and organized survey of the current state-of-the-art techniques for explainable 2D anomaly detection. By providing a refined taxonomy that accommodates the growing variety of techniques being developed, and realistic and inspiring future directions, this survey intends to give readers a thorough understanding of the various methods proposed for explainable 2D anomaly detection, including their advantages and disadvantages, and to assist them in finding the explainable anomaly detection technique most suited to their needs or a research topic they are interested in.

In summary, our paper presents several noteworthy contributions summarized as follows:

- We collect and summarize explainable methods in 2D anomaly detection tasks, and propose the taxonomy of these explainable methods.

- We compare these methods thoroughly, outline their advantages and disadvantages, and suggest some potential directions to address the existing drawbacks.
- We fill in the gaps for current surveys that give a brief introduction to the whole anomaly detection tasks but ignore the particularity of explainable methods in the 2D anomaly detection task.

The remainder of this survey is structured as follows. We first introduce the background of explainable 2D anomaly detection and some concepts in Sec. 2. Then, we summarize the existing methods for explainable 2D anomaly detection in Sec. 3. Next, we conclude the commons and differences of explainable image and video anomaly detection approaches in Sec. 4. We list the commonly used datasets for 2D visual anomaly detection in Sec. 5 and the standard evaluation metrics in Sec. 6. Finally, we point out potential directions for this topic in Sec. 7.

2 Background

2D anomaly detection pertains to the process of detecting abnormal patterns in images or videos. 2D anomaly detection approaches are usually trained on normal samples only and concentrate on learning the representation of anomaly-free data and detecting deviations from the learned model as anomalies. Based on the data type, 2D anomaly detection can be generally classified into image anomaly detection (IAD) and video anomaly detection (VAD).

Image anomaly detection

is of considerable significance in both academia and industry, with wide-range application scenarios including industrial inspection, medical health, and website management, etc. Image anomaly detection can be broadly classified into two sub-tasks: semantic anomaly detection (Salehi et al, 2021; Wang et al, 2022c; Tack et al, 2020; Reiss et al, 2021) and sensory anomaly detection in images (Bergmann et al, 2020; Venkataraman et al, 2020; Roth et al, 2022) and some approaches can possess both functions. For one-class classification, classification datasets, such as CIFAR-10 and CIFAR-100 (Krizhevsky et al, 2009), are usually employed to create a one-class

or leave-one-out setting or dataset-wise out-of-distribution setting. Tack et al (2020) put forward a distribution-shifting transformations-based contrastive learning scheme. Wang et al (2022c) seamlessly combine feature-level self-supervised learning with ad hoc feature adversarial perturbation for state-of-the-art performance. For both image-level anomaly detection and localization, the most commonly used dataset is MVTec AD (Bergmann et al, 2019). Bergmann et al (2020) pioneers image-level anomaly detection and segmentation through the disparity in output between the teacher and student models. More recently, Roth et al (2022) exploits an ImageNet-pretrained network for patch-level feature embedding extraction and proposes an effective core-set selection and representation distance calculation for anomaly score design, exhibiting the state-of-the-art performance so far.

Anomaly detection in videos

(e.g., surveillance videos) is a challenging yet significant task in multiple domains, such as public safety, healthcare, and ecology. The classic setting is that merely normal video clips are provided for training, and during testing the video sequences are composed of both normal and abnormal frames. The VAD algorithm is required to detect anomalous frames in testing. In the past few years, researchers have put lots of effort into enhancing video anomaly detection performance on standard datasets: UCSD Pedestrian (Mahadevan et al, 2010a), CUHK Avenue (Lu et al, 2013a) and ShanghaiTech Campus dataset (Liu et al, 2018). A popular branch of approach is the reconstruction-based methods which employ autoencoders for normal training data reconstruction and utilize reconstruction error as the anomaly score for test-time anomalous frame discrimination. For example, Hasan et al (2016) takes advantage of a deep convolutional network for spatio-temporal reconstruction-based VAD. Luo et al (2017) incorporates convolutional Long Short-Term Memory (Hochreiter and Schmidhuber, 1997) network into autoencoder for better consecutive frame temporal relationship modeling. In addition, Gong et al (2019) integrates memory with autoencoders for enhanced performance. Another prevailing type of method is the prediction-based approach. The rationale is

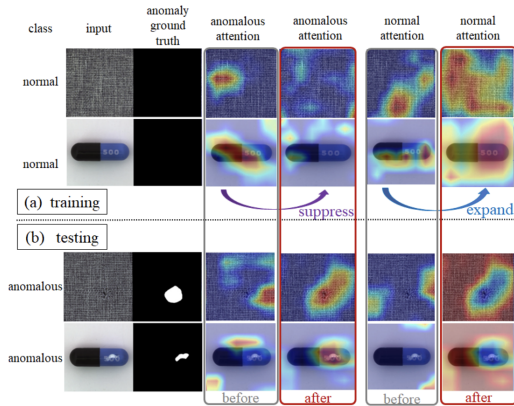


Fig. 1 Image from Venkataramanan et al (2020). The proposed CAVGA approach employs the complementary guided attention loss to force the attention map to cover all the normal regions and meanwhile suppress the anomalous attention on the normal images.

that the current frame is generated using preceding frames and the predictions with large error w.r.t. the true frames are considered anomalous. This concept is first proposed in Liu et al (2018) where U-Net (Ronneberger et al, 2015) is adopted as the architectural framework for frame prediction. A natural idea is to mix reconstruction-based techniques with prediction-based ones, resulting in hybrid methods (Tang et al, 2020; Liu et al, 2021). More recently, the approaches based on self-supervised learning have begun to dominate in VAD performance (Georgescu et al, 2021a; Ristea et al, 2022). Specifically, Georgescu et al (2021a) manually defines four pretext tasks for efficient learning of normal data patterns and Ristea et al (2022) proposes a masked dilated filter equipped with self-supervised reconstruction loss.

3 Explainable 2D Anomaly Detection

Explainable AI is essential to improving trust and transparency of AI-based systems (Adadi and Berrada, 2018). In anomaly detection, explainability is an ethical and regulatory requirement particularly in safety-critical domains (Li et al, 2023b; Ramachandra et al, 2020). We list the state-of-the-art explainable anomaly detection methods in images and videos in Tab. 1.

3.1 Explainable Image Anomaly Detection

For image anomaly detection, either semantic anomaly detection or pixel-level anomaly segmentation, explainability, and interpretability are of great significance to the understanding of why specific samples are considered anomalies and the development of more advanced approaches. Explainable image anomaly detection techniques can be broadly grouped into three kinds: Attention-based IAD, Input-perturbation-based IAD, and Generative-model-based IAD. The empirical result comparison on the public IAD benchmark MVTEC AD is provided in Tab. 2, where the Generative-model-based methods achieve the best performance.

Attention-based IAD

Attention in image recognition mainly refers to the concept that the model regards some parts or locations of a map or image as more important or interesting. Attention can be 1) post hoc (calculated with a trained model in hand), or 2) learned in a data-driven way. For the first type, the generated attention maps can be directly used to explain anomalies, as the high activation areas correspond to locations that the model pay more attention to and therefore indicate more abnormality. For instance, Liu et al (2020) generates attention from the latent space of a variational auto-encoder (VAE) through gradient calculation. Such attention maps can be adopted to detect anomalies in images. Also, Liznerski et al (2021) develops a Fully Convolutional Data Description method that maps the samples to an explanation attention map. There are some recent works that further take advantage of the post hoc attention to improve training. Venkataramanan et al (2020) makes use of the gradient-based attention to regularize the normal data training of the proposed convolutional adversarial VAE by proposing an attention expansion loss to enforce the attention map to concentrate on all normal parts. When having few anomalous training images in hand, they further put forward a complementary guided attention loss regarding the proposed binary classifier to refrain the network from focusing on erroneous areas. As illustrated in Fig. 1, such practice makes the network spare no effort to encode the normal patterns of the training images and

Table 1 Summary of explainable methods in 2D anomaly detection. “Type” represents in which way the method provides explanations. “Det.” and “Loc.” indicate whether the method can do anomaly localization (providing pixel-level scores) or simply can do detection (providing sample-level scores). For ODD works, we only list the testing out-of-distribution datasets.

Modality	Type	Year	Methods	Det. Loc.	Datasets	
Image	Attention	2020	GradCon (Kwon et al)	✓	C10, MN, fMN	
		2021	FCCD (Liznerski et al)	✓ ✓	fMN, C10, ImageNet, CURE-TSR	
	Input perturbation	2018	ODIN (Liang et al)	✓	TinyImageNet, LSUN, iSUN	
		2018	Mahalanobis (Lee et al)	✓	C10, SVHN, ImageNet, LSUN	
		2020	Generalized ODIN (Hsu et al)	✓	TinyImageNet, LSUN, iSUN, SVHN	
		2022	SLA ² P (Wang et al)	✓	C10, C100, Cal	
		2017	AnoGAN (Schlegl et al)	✓	Retina OCT	
	Generative model	2018	ALAD (Zenati et al)	✓	MN	
		2019	f-AnoGAN (Schlegl et al)	✓ ✓	UKB, MSLUB, BRATS, WMH	
		2019	Genomics-OOD (Ren et al)	✓	MN, SVHN	
		2020	Likelihood Regret (Xiao et al)	✓	MN, fMN, C10, SVHN, LSUN, CelebA	
		2021	FastFlow (Yu et al)	✓ ✓	MVTAD, BTAD, C10	
		2022	AnoDDPM (Wyatt et al)	✓ ✓	MVTAD	
		2022	Diffusion-anomaly (Wolleb et al)	✓ ✓	BRATS, CheXpert	
		2022	DDPM (Pinaya et al)	✓ ✓	MedMNIST, UKB, MSLUB, BRATS, WMH	
		2023	DiAD (He et al)	✓ ✓	MVTAD, VisA, BRATS	
		Foundation model	2023	WinCLIP (Jeong et al)	✓ ✓	MVTAD, VisA
			2023	CLIP-AD (Chen et al)	✓ ✓	MVTAD, VisA
			2023	AnomalyCLIP (Zhou et al)	✓ ✓	MVTAD, VisA, MPDD, BTAD, SDD, DAGM
			2023	SAA+ (Cao et al)	✓ ✓	MVTAD, VisA, KSDD2, MTD
2023	AnomalyGPT (Gu et al)		✓ ✓	MVTAD, VisA		
2023	Myriad (Li et al)		✓ ✓	MVTAD, VisA		
2023	GPT-4V (Cao et al)		✓	MVTAD, VisA, MVTLC, Retina OCT		
2023	GPT-4V-AD (Zhang et al)	✓ ✓	MVTAD, VisA			
Image+Video	Attention	2020	AD-FactorVAE (Liu et al)	✓ ✓	MN, MVTAD, Ped	
		2020	CAVGA (Venkataramanan et al)	✓ ✓	MVTAD, mSTC, LAG, MN, C10, fMN	
		2022	SSPCAB (Ristea et al)	✓ ✓	MVTAD, Ave, STC	
	Generative model	2019	LSAND (Abati et al)	✓ ✓	MN, C10, Ped, STC	
		2022	CFLOW-AD (Gudovskiy et al)	✓ ✓	MVTAD, STC	
Video	Attention	2020	Self-trained DOR (Pang et al)	✓ ✓	Ped2, Subway, UMN	
		2021	DSA (Purwanto et al)	✓ ✓	UCF, STC	
	Reasoning	2018	Scene Graph (Chen et al)	✓	UCF	
		2021	CTR (Wu and Liu)	✓	UCF, STC, XD	
		2023	Interpretable (Doshi and Yilmaz)	✓ ✓	Ave, STC	
		2024	VADor w LSTC (Lv and Sun)	✓	UCF, TAD	
		2017	JDR (Hinami et al)	✓ ✓	Ped2, Ave	
	Intrinsic interpretable	2021	XMAN (Szymanowicz et al)	✓ ✓	X-MAN	
		2022	VQU-Net (Szymanowicz et al)	✓ ✓	Ped2, Ave, X-MAN	
		2022	AI-VAD (Reiss and Hoshen)	✓	Ped2, Ave, STC	
2022	EVAL (Singh et al)	✓ ✓	Ped1, Ped2, Ave, STS, STC			

feedback-intensive responses in anomalous areas of images in the testing phase, accounting for why it outperforms the plain variants of autoencoders. Such explainable image anomaly detection methods usually compute the attention scores using functions similar to the Grad-CAM (Selvaraju et al, 2017), taking the form of

$$a_k = \frac{1}{M} \sum_i \sum_j \frac{\partial y}{\partial A_{ij}^k}, \quad (1)$$

where y can be any differentiable activation, A^k denotes the activations of feature map k , M is the total number of pixels in the feature map, i.e.

$$M = \sum_i \sum_j 1. \quad (2)$$

Kwon et al (2020) takes the first attempt to exploit backpropagated gradients as representations to design anomaly score function and puts

Table 2 Pixel-wise category-specific AUROC and mean AUROC for the MVTEC-AD dataset (Bergmann et al, 2019) of explainable IAD methods.

Category	Attention-based				Generative-model-based	
	AD-FactorVAE (2020)	CAVGA (2020)	FCDD (2021)	SSPCAB (2022)	FastFlow (2021)	CFLOW-AD (2022)
Carpet	0.78	-	0.99	0.950	0.994	0.9925
Grid	0.73	-	0.95	0.995	0.983	0.9899
Leather	0.95	-	0.99	0.995	0.995	0.9966
Tile	0.80	-	0.98	0.993	0.963	0.9801
Wood	0.77	-	0.94	0.968	0.970	0.9665
Bottle	0.87	-	0.96	0.988	0.977	0.9898
Cable	0.90	-	0.93	0.960	0.984	0.9764
Capsule	0.74	-	0.95	0.931	0.991	0.9898
Hazelnut	0.98	-	0.97	0.998	0.991	0.9889
Metal Nut	0.94	-	0.98	0.989	0.985	0.9856
Pill	0.83	-	0.97	0.975	0.992	0.9895
Screw	0.97	-	0.93	0.998	0.994	0.9886
Toothbrush	0.94	-	0.95	0.981	0.989	0.9893
Transistor	0.93	-	0.90	0.870	0.973	0.9799
Zipper	0.78	-	0.98	0.990	0.987	0.9908
Mean	0.86	0.93	0.96	0.972	0.985	0.9862

forward a novel directional gradient alignment constraint as part of the training loss function. For the second type of attention, Ristea et al (2022) introduces a channel attention mechanism after a masked convolutional layer for the reconstruction neural network design of the masked part of the convolutional receptive field. The proposed channel attention module is able to aggregate and recalibrate the feature information and selectively suppress reconstruction maps.

Input-perturbation-based IAD

In image-level anomaly detection tasks, input perturbation is a commonly adopted technique in both semantic anomaly detection (focusing on category difference) (Wang et al, 2022c) and out-of-distribution detection (focusing on dataset-wise distribution shift) (Liang et al, 2018; Hsu et al, 2020; Lee et al, 2018). In semantic anomaly detection, the training phase includes only data from a single class, termed the positive class. However, during the inference phase, the classifier deals with data from the positive class as well as data outside of it, which is sometimes called the negative class. The primary goal of semantic anomaly detection is to ascertain whether an item under examination belongs to the class that was represented during the training process (Perera et al, 2021; Khan and Madden, 2010). So basically the difference between anomalies and normal data lies in the semantic shift (i.e., they are from different categories). On the contrary, OOD detection aims to detect anomalies with covariate shift (Yang et al,

2021b), which means that the anomalous data are from different domains from the inliers. So in OOD detection, the standard benchmark setting is the training data is from one dataset (e.g. CIFAR-10) and the testing data is mixed by the training dataset and a new dataset from a different domain (e.g., CIFAR-10 and CIFAR-100). The OOD detection algorithm is expected to detect the data instances from the new dataset out. For both OCC and OOD detection, the input perturbation can be generally formalized as

$$x' = x + \text{perturbation term}, \quad (3)$$

where x denotes the input data or feature, and x' is the perturbed data or feature. The perturbation term is usually in the form of a perturbation magnitude multiplying the gradient of some score function w.r.t. the input. Then the perturbed data or feature serves as input for anomaly score calculation. Liang et al (2018) is the pioneering work adopting input perturbation technique in anomaly detection. The proposed ODIN method takes the gradient of a pretrained network and aims to increase the softmax score of any given input. Hsu et al (2020) generalizes ODIN via finding the maximum magnitude which maximizes the sum of the scores w.r.t. the in-distribution validation dataset. The generalized ODIN approach further enhances detection performance consistently. Instead of directly using softmax output scores, Lee et al (2018) proposes Mahalanobis

Table 3 Summary of the detailed perturbation formula in input-perturbation-based image anomaly detection task. ϵ denotes the perturbation magnitude, sign denotes the signum function, $S(x)$ is some score function of x and $D_{\text{in}}^{\text{val}}$ denotes the in-distribution validation set. The dashed line means that the first three methods utilize pre-trained classifier output for $S(x)$ while the last one uses a self-supervised learned classifier.

Method	Perturbation term	Magnitude ϵ	Score $S(x)$
ODIN (2018)	$-\epsilon \text{sign}(-\nabla_x \log S(x))$	searched	maximum softmax probability
Mahalanobis (2018)	$+\epsilon \text{sign}(\nabla_x S(x))$	searched	Mahalanobis distance-based confidence score
Generalized ODIN (2020)	$-\epsilon \text{sign}(-\nabla_x S(x))$	$\text{argmax}_{\epsilon} \sum_{x \in D_{\text{in}}^{\text{val}}} S(x)$	maximum softmax probability
SLA ² P (2022c)	$-\epsilon \nabla_x \log \bar{S}(x)$	searched	maximum softmax probability

distance-based confidence score, and the perturbation is introduced to enhance the confidence score. Different from these OOD detection work which computes the gradient using a pretrained network, Wang et al (2022c) trains a neural network with feature-level self-supervised learning and adds perturbation on the feature embeddings using the trained classifier network. The detailed comparison of the input perturbations of these literature is summarized in Tab. 3. Despite the differences among these input-perturbation methods, the rationale that they can explain anomalous patterns is the same: due to the characteristics of the anomaly detection problem anomalies are lower in quantity compared to the normal samples and the modes of anomalies are more diverse when applying the same amount of perturbation, the score alternations of them will be different from those of the normal data. Therefore we are able to examine the effect of output via input changes to generate reasonable explanations.

Generative-model-based IAD

Generative models (GM) are widely adopted in 2D anomaly detection. As summarized in Tab. 4, the most commonly used GMs include Generative Adversarial Networks (GAN), Autoregressive Models, Variational Autoencoders (VAE), Normalizing Flows, Diffusion Models and other variants of autoencoders. Schlegl et al (2017) is the first work to seamlessly combine GAN with image anomaly detection and localization task, where the reconstruction error of GAN and the discrimination score from the discriminator are jointly used for anomaly score design. This is because the GAN fails to reconstruct the anomalies well and the discriminator will regard the anomalies as fake since they only encounter normal ones in the training phase. Abati et al (2019) employs a deep autoencoder together with an autoregressive model for density estimation which learns

the distribution of the latent representations via maximum likelihood principles and proves empirically this is an efficient regularizer for anomaly detection. Furthermore, Ren et al (2019) demonstrates that likelihood from generative model-based anomaly detection methods is problematic due to the background statistics and proposes a novel likelihood ratio-based anomaly score. The key finding is that likelihood value is mainly controlled by the background pixels while likelihood ratios concentrate more on the semantic information, which explains why likelihood ratio is a more preferable choice for anomaly score for one-class classification. The formulation of the proposed likelihood ratio is

$$\text{LLR}(x) = \log p_{\theta}(x) - \log p_{\theta_0}(x), \quad (4)$$

where x is the data sample, $p_{\theta}(\cdot)$ is the model trained employing in-distribution data and $p_{\theta_0}(\cdot)$ is a background model which captures general background statistics. Similarly, Xiao et al (2020) addresses the problem that generative models, especially VAEs, are inclined to assign higher likelihoods on some types of OOD samples through defining a new OOD detection score dubbed as Likelihood Regret. They show that the Likelihood regret can be viewed as a specific form of log ratio of the likelihood from VAE. It is effective in separating anomalies out in that the increase of likelihood by substituting the model configuration with the optimal one for the single sample ought to be comparatively small for normal samples and large for anomalous ones thanks to the fact that the Variational AE is trained well on the normal training data.

$$\text{LR}(x) = L(x; \theta^*, \hat{\tau}(x)) - L(x; \theta^*, \phi^*). \quad (5)$$

Table 4 Summary of the generative-model-based image anomaly detection methods. Here CVPRW denotes CVPR Workshop. The abbreviations recon.error represents reconstruction error, disc.score represents discrimination score and recon.feature symbols reconstruction features respectively.

Method	Venue	Generative model type	Anomaly score function
AnoGAN (Schlegl et al)	IPMI 2017	Generative Adversarial Network	recon.error + disc.score
ALAD (Zenati et al)	ICDM 2018	Generative Adversarial Network	recon.error + disc.score
f-AnoGAN (Schlegl et al)	MIA 2019	Generative Adversarial Network	recon.error
LSAND (Abati et al)	CVPR 2019	Autoregressive Model	recon.error + likelihood
Genomics-OOD (Ren et al)	NeurIPS 2019	Autoregressive Model	likelihood ratio
AD-FactorVAE (Liu et al)	CVPR 2020	Variational Autoencoder	gradient-based attention map
Likelihood Regret (Xiao et al)	NeurIPS 2020	Variational Autoencoder	likelihood regret
FastFlow (Yu et al)	arXiv 2021	Normalizing Flow	likelihood
CFLOW-AD (Gudovskiy et al)	WACV 2022	Normalizing Flow	likelihood
AnoDDPM (Wyatt et al)	CVPRW 2022	Diffusion Model	recon.error
Diffusion-anomaly (Wolleb et al)	MICCAI 2022	Diffusion Model	recon.error
DDPM (Pinaya et al)	MICCAI 2022	Diffusion Model	recon.error
DiAD (Pinaya et al)	AAAI 2024	Diffusion Model	similarity

Here

$$L(x; \theta, \phi) = \mathbb{E}_{q_\phi(z|x)}[\log p_\theta(x|z)] - D_{\text{KL}}[q_\phi(z|x) \| p(z)] \quad (6)$$

represents the evidence lower bound, (ELBO), ϕ and θ are the parameters of the encoder and decoder respectively, ϕ^* and θ^* are the network parameters maximizing the population log-likelihood over the training dataset, and $\hat{\tau}(x)$ denotes the optimal parameter maximizing the ELBO of the test input x . (Liu et al, 2020) also utilizes VAE for anomaly detection, but instead uses a gradient-based attention map generated from the latent space of VAE for anomaly detection and localization in images. FastFlow (Yu et al, 2021) employs 2D normalizing flows for efficient and unsupervised anomaly detection and localization, providing explainability through intuitive visualizations of the transformed features for anomaly identification. CFLOW-AD (Gudovskiy et al, 2022) leverages conditional normalizing flows for unsupervised anomaly detection, offering explainability through the generative model’s ability to localize anomalies by contrasting reconstructed normal and anomalous regions, thereby enhancing the interpretability of detection results. More recently, diffusion models exhibit superior image generation ability and hence emerge in anomaly detection research. For example, AnoDDPM (Wyatt et al, 2022) proposes a partial diffusion strategy with simplex noise for medical image anomaly detection and localization. Wolleb et al (2022) integrates DDPM (Ho et al, 2020) with a binary classifier for medical image anomaly segmentation and Pinaya et al (2022) devises a

diffusion model for fast brain image anomaly segmentation. More recently, DiAD (He et al, 2023) develops a framework for detecting anomalies across multiple classes, integrating an autoencoder in pixel space, a semantic-guided network in latent space connected to the denoising network of the diffusion model, and a pre-trained extractor in the feature space, with innovations like spatial-aware feature fusion for enhanced reconstruction accuracy and semantic preservation. The critical advantage of the Diffusion Model for explainability is that each step in the forward step and reverse step has a closed form, which enables people to visualize the latent outputs of each step or layer in order to investigate how anomalies are ruled out in the diffusion process and where the model pay more attention.

Foundation-model-based IAD

With the recent rise of foundation model architectures, there exist several very recent works in image anomaly detection literature leveraging the extraordinary reasoning ability of large foundation models trained with massive amounts of data. There are a series of work using CLIP (Radford et al, 2021) (CLIPAD (Chen et al, 2023) ; (Zhou et al, 2023) AnomalyCLIP (Zhou et al, 2023); WinCLIP (Jeong et al, 2023); CLIP-SAM (Li et al, 2024)) for few-shot/zero-shot image anomaly detection and localization. More recently, Segment Any Anomaly (Cao et al, 2023b) introduces the "Segment Any Anomaly + (SAA+)" framework, a novel approach for anomaly segmentation under the zero-shot setting that utilizes hybrid prompt regularization to improve the

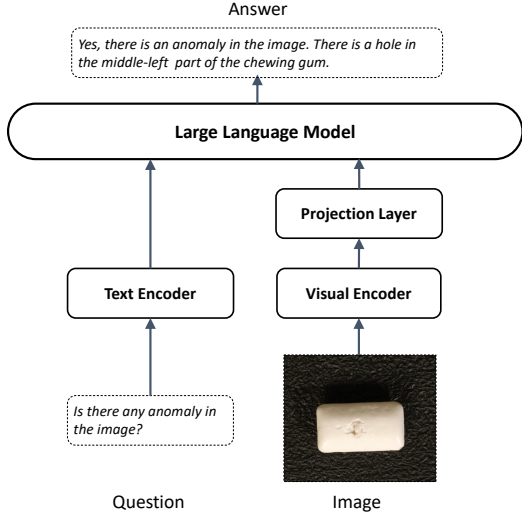


Fig. 2 Illustration of LLM-based image anomaly detection. A projection layer is usually applied after the extracted visual features to project them into the input token space of the LLM.

adaptability of foundational models. Instead of relying on domain-specific fine-tuning like traditional anomaly segmentation models, SAA+ leverages the zero-shot generalization capabilities of foundational models, assembling them to utilize diverse multi-modal prior knowledge for anomaly localization, and further adapts them using hybrid prompts derived from domain expert knowledge and target image context. The method’s explainability stems from its innovative use of hybrid prompts, which are derived from both domain expert knowledge and the specific context of the target image. The basic idea is to utilize the alignment property and extraordinary representation ability of text and visual features of CLIP for generic abnormality learning and discrimination, which makes the methods naturally explainable in the corresponding text prompt space. Nowadays, with the rapid development of LLMs and Large MultiModal Models (LMMs) (Yang et al, 2023), the outstanding reasoning ability of pre-trained language models has been employed for enhanced anomaly detection and explanations. AnomalyGPT (Gu et al, 2023) leverages LVLM for Industrial Anomaly Detection by simulating anomalous images with textual descriptions and fine-tuning LVLMs with prompt embeddings for direct anomaly presence and location assessment without manual thresholds. This approach

is explainable as it supports multi-turn dialogues, allowing users to engage with the model for detailed anomaly localization and understanding, facilitated by a lightweight decoder for fine-grained semantic capture and prompt learner integration for enhanced LVLM alignment. Myriad (Li et al, 2023a) introduces a novel large multimodal model, leveraging vision experts for enhanced industrial anomaly detection (IAD), which includes an expert perception module for embedding prior knowledge from vision experts and an expert-driven vision-language extraction module for domain-specific vision-language representation. This method enhances explainability by incorporating expert-generated anomaly maps into the learning process, thereby providing detailed descriptions of anomalies, which improves both detection accuracy and the comprehensibility of the detection process; Cao et al (2023c) tests the GPT-4V (Yang et al, 2023) capabilities in generic anomaly detection via examples, and Zhang et al (2023) adapts GPT-4V for zero-shot anomaly detection in images through granular region division, prompt designing, and text to segmentation, enhancing visual question answering for direct anomaly evaluation without prior examples. Its explainability stems from leveraging VQA to interpret and segment anomalies based on textual prompts and image analysis, providing intuitive and detailed anomaly identification and localization capabilities. All these existing LLM/LMM-based IAD methods are in the form of concatenation of the extracted text and image embeddings sent to LLM, as depicted in Fig. 2. Given a question related to the anomaly, the LLM can determine whether the image contains any anomaly, where it is, detailed descriptions, and even explanations. Owing to the massive knowledge the LLM is trained on, it can naturally generate meaningful textual explanations and further explanations can be acquired by changing or adding prompts.

3.2 Explainable Video Anomaly Detection

Explainability is a critical component in video anomaly detection. Currently, there is no particular definition of explainability in video anomaly detection. Also, it is not quantifiable. Thus, existing methods explain themselves by providing some

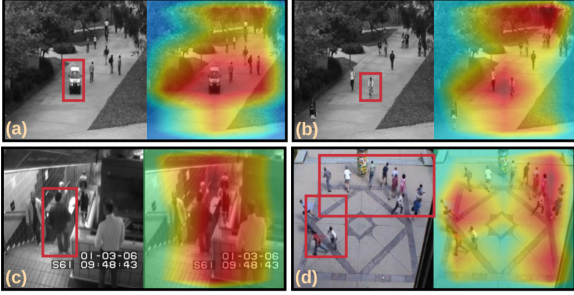


Fig. 3 Image from Pang et al (2020). Manually labeled anomalies in the original inputs (red rectangles on the left) and the corresponding CAM based saliency maps yielded by their method (right).

high-level ideas, such as anomaly localization, and action recognition, and some of them are intrinsically interpretable. In this section, we divide them into three main categories: Attention-based methods, Reasoning-based methods, and Intrinsic interpretable methods.

Attention-based methods

Attention-based methods are low-level explainable methods that give human insights into what a model is looking at. In other words, they highlight the pixels that contribute the most to the prediction. According to the attention map they produce, we can have a better idea of what specific areas do the model mainly focuses on and whether the area is aligned with human prior knowledge. In this case, it is very easy to troubleshoot the errors that the model makes. The typical process of attention-based methods is first to calculate the scores for anomalies in each frame, and then the attention-based method traces back from the anomaly score prediction to the activation map of raw frames. Specifically, the anomaly score estimation can be concluded as a sequential task, including the frame feature encoder and anomaly score function. Here we can formulate them as $S = f_{\theta}(X)$, where S indicates the anomaly scores and $X = \{x_1, x_2, \dots\}$ represents the sequential frames, and $f_{\theta}(\cdot)$ means the combination of feature encoder and the anomaly score function. Calculating the anomaly scores can be done in various ways. However, to achieve attention-based interpretability, the key is to adopt the activation map from the anomaly scores. In the context of the given frame x , the $p_k(i, j)$, denoting the activation value of a unit indexed by k within the last

layer, localized at the spatial coordinates (i, j) . Concurrently, the symbol w_k is designated to represent the weight linked to unit k in relation to the computation of the anomaly score. $\phi(x)$ is defined as the attention score of a frame which can be expressed as:

$$\phi(x) = \sum_{i,j} \sum_k w_k \cdot p_k(i, j). \quad (7)$$

This formulation encapsulates the interplay between the activation values, their associated weights, and the resultant anomaly score, forming a fundamental construct within the framework.

The key idea of attention-based methods is to capture the gradient. How to calculate the gradient and how to use them to explain the model are the novel parts of this kind of method. Pang et al (2020) used a simple approach, class activation mapping (CAM) (Zhou et al, 2016), to calculate attention weights. They then localized the identified anomaly by looking at high activation values on the attention map. Purwanto et al (2021) used a self-attention mechanism to model the relationships of the nodes in spatio-temporal graphs. They construct conditional random fields as nodes and learn self-attention on them. Visualization of the heat map on the self-attention random fields reveals the location of the anomaly. Other papers, such as Venkataramanan et al (2020), also use attention to localize the anomaly and give an explanation based on that. Although the attention map indicates the importance of a specific region or features that play a significant role in the prediction, it cannot explain why a model makes a correct or wrong prediction. For example, in Fig. 3, the attention map indicates a larger region than the anomaly, which reveals little information. Also, as Cao and Wu (2022) discussed, a random ResNet can provide an attention map that can capture the foreground object. In this case, it can tell nothing even if it gives an accurate prediction.

Reasoning-based methods

Different from the attention-based method, reasoning-based methods focus on giving high-level explanations by providing some context reasoning techniques, such as knowledge graph, scene graph, and causal inference. They explain the model in a semantic way that considers the foreground objects and the background information

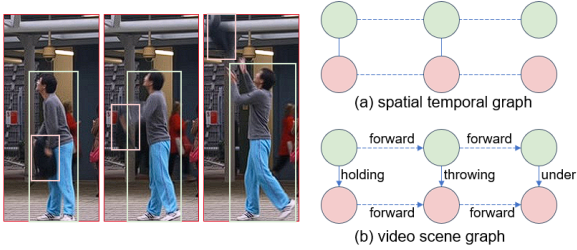


Fig. 4 Illustration of (a) spatial-temporal graph and (b) video scene graph generation using consecutive frames from the Avenue dataset. Both graphs capture valuable semantic information regarding objects. In the spatial-temporal graph, objects with overlapping bounding boxes are connected by spatial edges. Temporal edges indicate consecutive frames for a given object, effectively incorporating temporal information. These edges also encode semantic details, such as bounding box distances. In the case of video scene graphs, (subject, predicate, object) triplets are employed to articulate relationships between objects. This enables the description of frames in a semantically meaningful manner. For instance, (man, hold, bag) represents the initial frame, which then transitions to (man, throw, bag), and eventually (man, under, bag). These changing relations offer a high-level explanation of anomalies within the scene.

together. As shown in Fig. 4, the frame information can be formulated as graphs, including spatial-temporal graph, knowledge graph, scene graph, and so on. The information provided by graph can not only benefit anomaly detection but also bring interpretability to models.

For example, [Doshi and Yilmaz \(2023\)](#) proposed a framework with a global monitor and a local monitor. The global monitor constructs a scene graph that captures the global information, and the local monitor focuses on the human pose. Each interaction is observed by calculating its semantic distance from a collection of nominal embeddings derived from the training data. Typically, the (subject, predicate, object) triplet is mapped to numerical vectors using a semantic embedding network. The goal of metric learning is to extract information regarding the absence or presence of anomalies from the interaction embeddings. During training, the positive instance is randomly selected from the nominal training set, and the negative instance is randomly sampled from an artificially generated set of anomalous interaction triplets, e.g., a person hits a person. The objective is to minimize the distance between the positive samples and to maximize the negative samples. Thus, during testing, when an

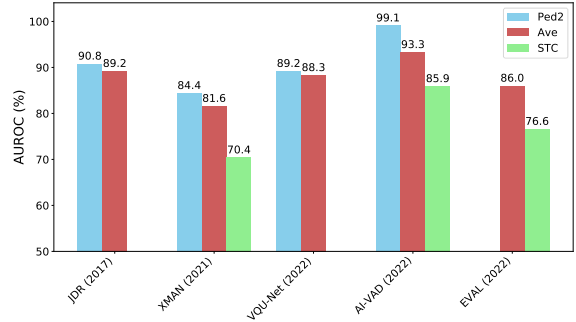


Fig. 5 Video anomaly detection performance of Intrinsically interpretable methods on Ped2, Ave, and STC datasets under the semi-supervised setting.

anomaly occurs, it can give the true reason for the anomaly and output an interpretable result. Similarly, [Chen et al \(2018\)](#) also relied on scene graphs to interpret the anomaly. However, it took advantage of multiclass SVM and naive Bayesian for anomaly detection.

The knowledge graph can also capture semantic information. [Nesen and Bhargava \(2020\)](#) constructed a knowledge graph by aligning prior knowledge and recognized objects, which provides a semantic understanding of a video. For example, a supercar in a poor district is an anomaly event. Techniquely, the relationship between the ontologies of the knowledge graph and objects detected in a video is determined by calculating the similarity between entities present in the frame. In addition, causal inference is born to explain models. [Wu and Liu \(2021\)](#) proposed a module for causal temporal relations to capture the temporal cues between video snippets, which simultaneously explores two types of temporal relationships: semantic similarity and positional prior. Reasoning-based methods provide high-level explanations that are similar to human understanding. However, it is more complicated and requires high-quality object recognition model in the first place. In other words, it will fail if an object is misclassified.

Intrinsically interpretable methods

Intrinsically interpretable methods are the dominant explainable way in video anomaly detection, with strong empirical performance on benchmark datasets as illustrated in Fig. 5. They can be further classified into two categories: a) post-model

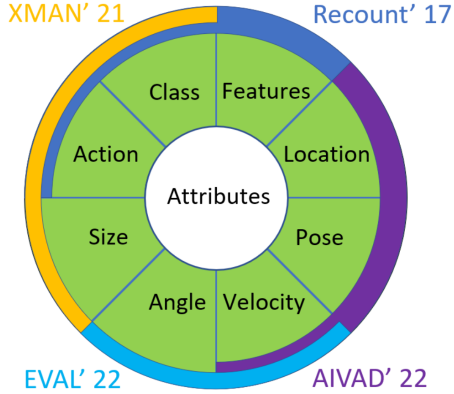


Fig. 6 Visualization of the attributes that are applied in existing methods. Those attributes are object-level. Class indicates the object category, like person, bag; features indicate the feature of an object, such as white, young and size refers to the size of the bounding box.

interpretable methods, and b) in-model attributes interpretation methods. Post-model interpretable methods explain anomalies by analyzing differences between the actual values and the predictions of the model. These differences reveal normal patterns that the model learns and the abnormal events that diverge from normal videos. In fact, most reconstruction-based or prediction-based methods have explainability to some degree and belong to post-model interpretable methods. This procedure can be formulated as:

$$\phi(x) = \theta(f(x) - x), \quad (8)$$

where $\phi(\cdot)$ shows the heat map of each frame, and $f(\cdot)$ denotes the prediction frame and x is the ground truth frame, and $\theta(\cdot)$ represents the projection of difference of prediction and groundtruth. For example, [Szymanowicz et al \(2022\)](#) trained a neural network for predicting future frames. The predicted frame is compared to the ground truth frame and results in a pixel-level error map. Notably, although the error map looks like the saliency map or attention map, they are essentially different. The attention map reveals the weight of each pixel, while the error map indicates the prediction error based on each pixel. Based on the error map, it is easy to locate the error region. The object classification and action recognition models are applied to classify and explain the anomalies.

On the other hand, attribute interpretation methods make use of object attributes to determine whether an object is normal or abnormal.

As illustrated in Fig. 6, most of them adopt attributes that are based on prior knowledge, such as velocity, pose, motion, action, and location. For example, [Singh et al \(2022\)](#) proposed a framework that extracts a high-level depiction of each video segment utilizing networks for appearance and motion. They choose the motion angle and velocity as the attributes to help explain the model. The method for selecting exemplars is applied to choose a representative subset of video segments for a specified spatial region, whose object and its corresponding angle and velocity are kept in the memory bank. During testing, a video sequence is classified as an anomaly if it is different from exemplars. Thus, the explanation can be made by the high-level representation. In particular, the appearance and motion parts of the combined feature vector are mapped to high-level attributes using the last fully connected layer of their respective networks. There are some other papers using different attributes. [Hinami et al \(2017\)](#) considered object class and corresponding features and actions. They judge anomaly by predicting anomaly scores of each visual concept. The reason the anomaly can be inferred from these concepts is if one concept is largely deviating from normal patterns. [Reiss and Hoshen \(2022\)](#) regard velocity, pose, and deep as attributes to interpret anomaly. Similarly, these features provide predictions and explanations for anomalies. [Szymanowicz et al \(2021\)](#) paid more attention to interactions, so they encoded object category, interaction, and size of bounding box and trained a Gaussian Mixture Model (GMM) from these representations.

In summary, intrinsically interpretable methods can give straightforward explanations without many complicated operations. Although they cannot give some high-level ideas like reasoning-based methods, object attributes perspective is able to explain most anomalies. However, it is important to choose features manually, which requires the human understanding of a particular dataset.

4 Differences and Commons

4.1 Explainable methods that can only be exclusively applied to images

From a feasibility perspective, the image anomaly detection methods can be applied to video data

as well due to the fact that a video is a sequence of images in essence. Nevertheless, considering the intrinsic characteristics of the video anomaly detection task, many of them are not able to work reasonably on the benchmark video anomaly detection datasets.

The input-perturbation-based image anomaly detection approaches that utilized pretrained classification models (Liang et al, 2018; Hsu et al, 2020; Lee et al, 2018) can not work on video anomaly detection tasks. They can be applied to the tasks of video anomaly detection in a frame-wise fashion, but image classification dataset-pretrained networks fail to differentiate between normal and abnormal frames in that the abnormality in video anomaly detection lies in detailed frame patch abruptness or intra-frame variation. These can not be represented by pre-trained image classification models which concentrate more on the categorical information. There is a line of video anomaly detection works that perform video detection of anomalies at the level of individual objects, and it seems that the input-perturbation-based image anomaly detection approaches can be incorporated into them. Nevertheless, such techniques fail to detect anomalies that result from intra-frame variation, which occupies a large proportion of all the anomalies, including people running, skating, falling, fighting, etc. This is because the essence of such kind of anomaly is the relative alternation across the frames, not the object category difference.

For image OOD detection methods using generative models including Ren et al (2019); Xiao et al (2020), they learn the density function of the in-distribution data so that the likelihood-related score will be lower for outliers. Such methods certainly can not work for video anomaly detection owing to the fact that they can neither distinguish between unseen object category and seen object category nor model the variation across frames.

In summary, an explainable image anomaly detection method can be adapted for videos only if they have an error-based anomaly score. The video data can be concatenated in channel dimension to feed into the model and the error-based score can still detect anomalies in video frames, either object anomalies or motion anomalies.

4.2 Explainable methods that can only be exclusively applied to videos

Video anomaly detection has primarily focused on detecting anomalies in actions. As a result, video-explainable methods have emerged to provide explanations by leveraging video-specific features, such as temporal information and action information. These model-specific explainable methods are tailored to videos, as images lack the contextual cues necessary for such analysis. Conversely, reasoning-based explainable methods heavily rely on the contextual information inherent in videos. For instance, scene graphs have been employed as a general tool to analyze object relationships. However, image anomaly detection suffers from the inherent limitation of having only a few objects present, thereby limiting the scene graph’s capacity to provide meaningful explanations for predictions due to the lack of context.

In order to address this limitation, Doshi and Yilmaz (2023) have proposed a novel approach that constructs a scene graph capable of capturing global information. The authors utilize a semantic embedding network to map (subject, predicate, object) triplets to numerical vectors. Through metric learning, the aim is to extract information pertaining to the absence or presence of anomalies from the interaction embeddings. During testing, when an anomaly occurs, this approach enables identifying the true cause of the anomaly and producing an interpretable result.

Another key aspect specific to videos is the temporal sequence. Many video anomaly detection methods (Yu et al, 2020; Wang et al, 2022b; Liu et al, 2021) make use of both the RGB frame cube and the optical flow cube. The optical flow cube provides crucial temporal and action context that is not available in individual images. By leveraging this information, several explainable methods have explored temporal sequences to generate interpretable results.

In summary, video anomaly detection research has witnessed advancements in explainability techniques. While model-specific explainable methods rely on video-specific features, such as temporal and action information, reasoning-based explainable methods require contextual cues present in videos. The construction of scene graphs capturing global information and the exploitation

of temporal sequences through optical flow analysis have further enhanced the interpretability of video anomaly detection approaches.

4.3 Commons

All the error-based image anomaly detection methods can be flexibly adapted to video anomaly detection tasks. The practice is simple: for a video $X \in \mathbb{R}^{T \times C \times H \times W}$, where T denotes the video clip length, C denotes the channel number and H, W represents the height and width of the frames respectively. Then we can simply reshape the video tensor by concatenating the channel dimension across the frame level, then we have $X' \in \mathbb{R}^{TC \times H \times W}$ and we are able to view it as an image and apply the image anomaly detection method. The rationale that they can still work is that the error-based score usually presents in the form of the subtraction between input and the reconstruction output in some form, so for the object anomaly, the error is certainly discriminative and for the motion anomaly, the error is still discriminative. More concretely, for appearance (object) anomalies in video anomaly detection, including unseen vehicles, skateboards, bicycles, etc., the error score in each frame is discerning, therefore the summation of them across the temporal dimension is still discerning. In this case, the error gap mainly exists at the spatial level. For motion anomalies, despite the fact that looking at each frame individually, the error score might not be that discriminative since the objects may have been witnessed during training (people). Nevertheless, the variation of the pixel values along the time axis has not been seen during the training, so the error gap considering all the consecutive N frames will be large. In this case, the error gap mainly exists at the temporal level. We illustrate such practice and phenomenon in Fig. 7.

It is noteworthy that the error-based score not necessarily take advantage of the reconstruction error. As long as the error-based score accumulates the error over the spatial dimension in some form, it can be easily adapted to video tasks, including reconstruction-error-based score (Liu et al, 2020; Venkataramanan et al, 2020; Ristea et al, 2022; Abati et al, 2019), log-likelihood score (Abati et al, 2019), Dice score (Wolleb et al, 2022; Pinaya et al, 2022) and reference discrimination score using GAN (Schlegl et al, 2017). We can also introduce a

more refined design along the temporal dimension for better time variation information excavation when adjusting such approaches to video data and we leave this for future work.

Similarly, the attention-based explainable method can be utilized for image anomaly detection. Although the video has a temporal dimension, most methods (Pang et al, 2020; Venkataramanan et al, 2020) regard a frame cube as a single object. For example, for a video $X \in \mathbb{R}^{T \times C \times H \times W}$, the sample of a cube has dimension $\mathbb{R}^{C \times H \times T \times W}$. In this case, the video sequence can be converted to a large image which actually concatenates several frames. The attention map can thus reflect the predicted anomaly location and visualized weights of each pixel.

Some intrinsic methods (Szymanowicz et al, 2021; Hinami et al, 2017) can also be transferred to image anomaly detection. The key idea of the intrinsic method is to leverage its own attributes to explain the prediction. For example, Szymanowicz et al (2021) generated three representations of object category, interaction, and size of bounding box and trained a Gaussian Mixture Model (GMM) using these representations. It can explain itself by telling which part is deviated from the normal distribution. Hinami et al (2017) trained three classifiers to classify one’s category, action, and attributes. Although these classifiers are not involved in detecting anomalies, they can show why an object is abnormal afterward. However, as we know, image anomaly detection may not have such attributes as interaction, or motion. Object category usually is not meaningful as the image anomaly detection task has the same object type. Although these video-specific attributes cannot be transferred to images, images themselves have their own attributes, like size, and shape. This additional prior information is helpful to explain the anomaly in a semantic way. Explainable methods in image anomaly detection can definitely adapt a similar procedure to explain the results using image-specific attributes. Besides, some perturbation methods can also adopt such feature embeddings. For example, Wang et al (2022c) perturbed some feature embeddings by the corresponding classifiers.

Foundation-model-based IAD approaches, especially the LLM-based ones can be easily adapted and applied to video data. The difference is that for video anomaly detection, the input

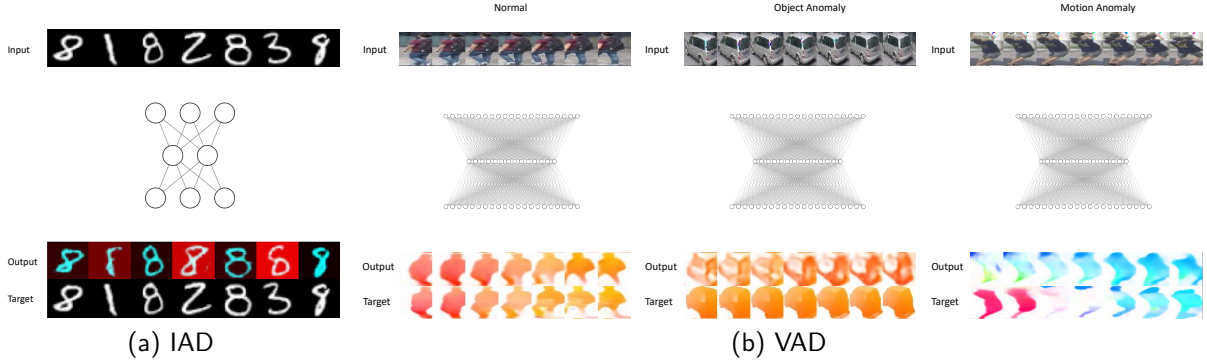


Fig. 7 Error-based anomaly detection methods work for both image and video data. (a) Schematic diagram of error-based image anomaly detection example adapted from [Perera et al \(2019\)](#). The error is the distance between the input image and the reconstruction and is minimized during training. The training data are all number 8s, which are the normal samples. In the inference face, the error will be small for 8s but large for other numbers. (b) Schematic diagram of error-based video anomaly detection example with a window length of 7 adapted from [Wang et al \(2022b\)](#). The consecutive frames can be concatenated in channel dimension and then sent into the network for reconstruction. The example here shows the motion branch approach ([Wang et al, 2022b](#)), where the input is raw frames, and the target is the corresponding optical flow maps. The outputs of the network are required to be close to the target optical flows during training. During the training, all samples are normal data containing normal behavior of pedestrians like walking. During the testing, when encountering normal samples (first column: a walking person), the total error can be minimal since each frame’s reconstruction closely approximates the target images. For object anomaly (second column: an unseen object like a car), the reconstruction error of every frame will be large, which shares the same mechanism as error-based image anomaly detection, leading large total error. For motion anomaly (third column: a person catching a dropping bag while looking upwards), the reconstruction error of certain few frames can be small (last three here), but due to the abruptly changing motion, there must be some frames with extraordinarily large error (first four here), leading to a relatively large error in total.

visual data has an additional temporal dimension, which can be processed by pooling ([Maaz et al, 2023](#)) or learning modules ([Lv and Sun, 2024](#); [Wang et al, 2023](#)) to eliminate the temporal dimension and sent into LLM after concatenation with prompt features. The input token space is inherently capable of handling the temporal relationship of the video frames, making the whole anomaly detection pipeline transparent and interpretable.

5 Datasets

In this section, we summarize the most widely used public datasets for 2D anomaly detection, which contributes to the understanding of the explainabilities of the methods applied to them.

5.1 Image Anomaly Detection

For OOD detection and semantic anomaly detection works of image anomaly detection, the experiments are usually conducted on image classification datasets by setting some class(es) as normal data and the remainder as abnormal data. The commonly used classification datasets

include CIFAR-10 (C10) ([Krizhevsky et al, 2009](#)), CIFAR-100 (C100) ([Krizhevsky et al, 2009](#)), MNIST (MN) ([LeCun et al, 1998](#)), Fashion-MNIST (fMN) ([Xiao et al, 2017](#)), Texture ([Kylberg, 2011](#)), LSUN ([Yu et al, 2015](#)), Caltech-101 (Cal) ([Fei-Fei et al, 2004](#)), CURE-TSR ([Temel et al, 2017](#)), iSUN ([Xu et al, 2015](#)), SVHN ([Netzer et al, 2011](#)) and CelebA ([Liu et al, 2015](#)) etc. The types of explainable IAD methods corresponding to the aforementioned datasets are mainly input-perturbation-based and generative-model-based methods, which concentrate on sample-level discriminativity. So in the following IAD datasets listed, we mainly focus on sensory anomaly detection/localization datasets, which are mostly applicable to attention-based, generative-model-based, and foundation-model-based IAD approaches.

MVTec AD (MVTAD) ([Bergmann et al, 2019, 2021](#))

presents an extensive dataset designed for unsupervised anomaly detection within natural imagery. This dataset simulates real-world scenarios encountered in industrial inspections and

includes 5,354 high-resolution pictures showcasing five distinct textures and ten different objects from various fields. The data set includes 73 different types of anomalies that present as defects or structural changes in objects or their textures. For every image containing a defect, it offers pixel-precise ground truth areas, which enable the assessment of techniques for both anomaly identification and segmentation.

MVTec LOCO AD (MVTLC) (Bergmann et al, 2022)

presents a novel dataset aimed at assessing the performance of unsupervised algorithms for localizing anomalies. This dataset comprises 3,644 images across five unique object categories, modeled after real-world industrial inspection settings. The anomalies within the dataset are categorized into structural and logical types. It clearly differentiates between structural anomalies, which are described as physical defects like scratches, dents, or impurities, and logical anomalies, which are characterized by violations of inherent rules, such as an object being misplaced or missing entirely.

VisA (Zou et al, 2022)

is a comprehensive collection of 10,821 images, featuring 9,621 normal and 1,200 anomalous samples across 12 subsets corresponding to different objects, including complex printed circuit boards (PCB) and simpler objects like Capsules, Candles, and various food items. These subsets capture a range of conditions, from multiple instances with varied poses and locations to roughly aligned objects, with anomalies such as surface and structural defects meticulously introduced to simulate realistic conditions. The dataset, captured with a high-resolution RGB sensor, provides both image and pixel-level annotations for detailed analysis.

Fishyscapes (Blum et al, 2019)

serves as a public standard for gauging uncertainty in the practical task of semantic segmentation related to urban driving. It assesses the accuracy of pixel-level uncertainty predictions in identifying unusual objects in the vehicle’s path. It is the first public benchmark specifically designed for anomaly detection in a real-world task of

semantic segmentation for urban driving scenarios. The benchmark reveals that anomaly detection remains a challenging task, even in common situations. The Fishyscapes dataset is based on data from Cityscapes (Cordts et al, 2016), a well-known benchmark for semantic segmentation in urban driving. The benchmark comprises two main components: Fishyscapes Web, where Cityscapes images are overlaid with objects sourced from the web, and Fishyscapes Lost and Found, which builds on a road hazard dataset collected similarly to Cityscapes.

RoadAnomaly21 (Chan et al, 2021)

significantly enhances anomaly segmentation in street scenes by offering an evaluation dataset of 100 images, each with detailed pixel-level annotations. This dataset, an expanded and refined version of a prior collection, features a more diverse set of images with improved quality and more precise labeling, including the addition of a void class and 68 new images. It rigorously removes low-quality images and corrects previous labeling errors, ensuring a clear focus on road scenes. Each image in the dataset showcases at least one anomalous object, such as unexpected animals or unidentified vehicles, sourced from a variety of web-based environments to ensure a wide diversity in object sizes, locations, and scene types. To aid in method validation, the dataset also includes 10 extra images with annotations, allowing users to test the compatibility of their approaches with this benchmark.

LAG (Li et al, 2019)

, a large-scale glaucoma detection dataset, features 5,824 fundus images (2,392 positive and 3,432 negative for glaucoma) from Beijing Tongren Hospital, evaluated under the Helsinki Declaration guidelines and exempt from patient consent due to its anonymized nature. Each image has been rigorously diagnosed by specialists using both morphologic and functional analyses, establishing a gold standard for glaucoma detection.

UK Biobank (UKB) (Sudlow et al, 2015)

is a vast and comprehensive prospective study initiated between 2006 and 2010, enrolling over 500,000 participants aged 40–69 years, aimed at

investigating the genetic and environmental determinants of diseases prevalent in middle and old age. It encompasses a wide array of data including phenotypic and genotypic information, physical measurements, and longitudinal health outcomes, making it a valuable resource for public health research accessible to researchers worldwide.

MSLUB (Lesjak et al, 2018)

comprises MRI images of 30 Multiple Sclerosis patients, featuring white-matter lesion segmentations validated through a multi-rater consensus. This dataset, designed for the creation and testing of automated lesion segmentation methods, emphasizes the use of semi-automated tools to reduce variability both within and between different raters, aiming to enhance the accuracy and reliability of MS lesion identification and quantification in clinical settings.

Brain Tumor Segmentation (BRATS) (Menze et al, 2014)

is designed for the assessment of cutting-edge techniques in segmenting brain tumors using multi-parametric MRI imaging. The collection features pre-operative MRI scans from multiple institutions focused on glioma tumors. It underscores the delineation of different tumor sub-regions and the forecasting of patient survival outcomes, utilizing radiomic features and ML techniques.

White Matter Hyperintensities (WMH) (Kuijf et al, 2019)

provides a standardized framework for the automatic segmentation of white matter hyperintensities from multi-center, multi-scanner brain MRI data, aiming to facilitate the development and comparison of segmentation methods. It includes 60 training images with manual segmentations and a test set of 110 images, evaluated on metrics like Dice similarity coefficient and sensitivity, to validate segmentation algorithms' performance across different MRI scanners and protocols.

CheXpert (Irvin et al, 2019)

is a large public collection of 224,316 chest radiographs from 65,240 patients, labeled for the presence of 14 observations as positive, negative, or uncertain. It includes an innovative approach to capture uncertainties in radiology reports

through automatic labeling, facilitating research into developing algorithms for chest radiograph interpretation that effectively handle uncertainty.

MedMNIST (Yang et al, 2021a)

is a collection of 10 pre-processed medical image datasets, designed for classification tasks with lightweight 28x28 images, aiming to facilitate educational purposes, rapid prototyping, and AutoML benchmarks in medical image analysis. It includes diverse data scales and tasks across primary medical image modalities, making it accessible for multi-modal machine learning challenges without extensive background knowledge.

KSDD2 (Božič et al, 2021)

consists of over 3,000 high-quality images capturing various types of defects on production items, designed to propel advancements in the detection of surface defects within industrial environments. This dataset, enriched with fine-grained segmentation masks for precise defect localization, represents a significant resource for developing and benchmarking image analysis algorithms for real-world industrial quality control challenges.

Magnetic Tile Defect (MTD) (Huang et al, 2020)

focuses on the real-time detection of surface defects on magnetic tiles using the MCuePush U-Net model, combining MCue U-Net and Push network for enhanced defect localization. It significantly improves the speed and accuracy of defect detection in industrial settings, reducing inspection time from 0.5s per image to 0.07s while offering state-of-the-art performance for identifying defects through deep learning techniques.

SDD (Tabernik et al, 2020)

is designed for the segmentation and detection of surface defects, utilizing a deep learning architecture optimized for this task. It is distinguished by its efficiency in learning from a limited number of defective samples, demonstrating its practicality for industrial applications where only a few defective examples may be available for training.

BeanTech Anomaly Detection (BTAD) (Mishra et al, 2021)

is a collection of 2,830 real-world industrial images of three different products, designed for anomaly detection tasks. It features both normal and defective product images, with the defective ones being manually labeled for pixel-wise ground-truth anomaly localization, facilitating the development and evaluation of anomaly detection and localization algorithms.

DAGM (Wieler and Hahn, 2007)

was created for the DAGM 2007 competition, focusing on weakly supervised learning for industrial optical inspection. It is designed to challenge and benchmark algorithms in the area of visual defect detection on various manufacturing materials, emphasizing the importance of pattern recognition and machine learning techniques in industrial quality control.

MPDD (Jezek et al, 2021)

addresses the challenge of defect detection in metal fabrication and painting, focusing on the variability and complexity of real-world manufacturing conditions. It aims to improve the performance of semi-supervised and unsupervised anomaly detection methods by providing a dataset that includes a variety of metal parts under different conditions, highlighting the need to test anomaly detection methods in diverse, application-specific scenarios for development and accuracy enhancement in industrial settings.

5.2 Video Anomaly Detection

In this section, we introduce some popular datasets for video anomaly detection and give some insight on whether it can be applied to different explainable methods. The detailed statistics of the listed datasets are given in Tab. 5, which, for the first time, lists the anomaly classes of each dataset for a better understanding of their nature.

UMN (Raghavendra et al, 2006)

contains a series of video clips that are recorded from different scenes, such as an indoor hallway, an outdoor lawn, and a plaza. The abnormal events are characterized by people suddenly starting to run in all directions, simulating an escape or panic

scenario. However, it does not provide object-level anomaly labels, which limits its use in evaluating explainable video anomaly detection models.

UCSD Pedestrian 1 (Ped1) (Mahadevan et al, 2010b)

includes video segments showing crowds moving and walking. It comprises 34 training video samples and 36 testing video samples. Additionally, a subset of 10 Ped1 clips is provided with hand-crafted binary masks at the pixel level, which serve to pinpoint areas that contain anomalies. This feature enables the evaluation of an algorithm’s ability to localize anomalies. The inclusion of mask regions facilitates the assessment of explainability through the anomaly localization task.

UCSD Pedestrian 2 (Ped2) (Mahadevan et al, 2010b)

contains 16 training and 12 test videos. It is meticulously crafted to comprehensively encompass a broad spectrum of anomalous activities such as unauthorized vehicles, bicycles, skateboarders, and wheelchairs intruding into pedestrian regions. Notably, these datasets are celebrated for not only their complexity but also for embodying a wide range of real-world scenarios, thereby serving as a robust platform for the explainability of advanced anomaly detection algorithms, and catalyzing research towards innovative solutions for recognizing and addressing anomalies in dynamic, pedestrian-rich environments. The dataset is very suitable for attention-based explainable method, but due to the lack of detailed attributes, it cannot apply to the attribute-based explainable methods.

Subway (Adam et al, 2008)

encompasses two videos, including a 96-minute entrance gate segment and a 43-minute exit gate clip. It offers a rich tableau of both regular and irregular passenger behaviors within a bustling subway environment. Anomalies are typified by passengers moving in erroneous directions and ticket evasion attempts, presenting a robust and challenging testing ground for the creation and assessment of anomaly detection algorithms in real-world, high-density transit scenarios. The dataset is very suitable for attention-based explainable methods but similar to Ped2,

Table 5 Comparisons of different Video Anomaly Detection datasets. The UMN dataset does not have official training and testing splits. The UBnormal dataset includes a validation set, which is not displayed here. For setting, “Se” denotes Semi-supervised, “We” denotes Weakly-supervised and “Su” denotes Supervised.

Dataset	Year	Setting	#Scenes	# Frames			# Anomaly classes	Anomaly classes
				Total	Training	Testing		
Subway Entrance (Adam et al)	2008	Se	1	144,250	76,453	67,797	5	Loitering, Wrong direction, Illegal exit, Unattended objects, Crowding
Subway Exit (Adam et al)	2008	Se	1	64,901	22,500	42,401	3	Wrong direction, Illegal exit, Unattended objects
UMN (Raghavendra et al)	2009	Se	3	7,741	-	-	1	Escaping panic
USCD Ped 1 (Mahadevan et al)	2010	Se	1	14,000	6,800	7,200	5	Biking, Skating, Small carts, People in wheelchair, People walking across a walkway or in the grass that surrounds it
USCD Ped 2 (Mahadevan et al)	2010	Se	1	4,560	2,550	2,010	5	Biking, Skating, Small carts, People in wheelchair, People walking across a walkway or in the grass that surrounds it
CUHK Avenue (Lu et al)	2013	Se	1	30,652	15,328	15,324	5	Running, Loitering, Throwing objects, Wrong direction, Gathering
ShanghaiTech (Zhang et al)	2017	Se	13	317,398	274,515	42,883	11	Biking, Running, Loitering, Vehicle, Skateboarding, Climbing, Throwing objects, Fighting, Jaywalking, Gathering, Abnormal Object
UCF-Crime (Sultani et al)	2018	We	-	13,741,393	12,631,211	1,110,182	13	Abuse, Arrest, Arson, Assault, Road Accident, Burglary, Explosion, Fighting, Robbery, Shooting, Stealing, Shoplifting, Vandalism
XD Violence (Wu et al)	2020	We	-	18,748,800	-	-	6	Abuse, Car accident, Explosion, Fighting, Riot, Shooting, Jaywalking, Biker outside lane, Loitering, Dog on sidewalk, Car outside lane, Worker in bushes, Biker on sidewalk, Pedestrian reverses direction, Car u-turn, Car illegally parked, Person opening trunk, Person exits car on street, Skateboarder in bike lane, Person sitting on bench, Metermaid ticketing car, Car turning from parking space, Motorcycle drives onto sidewalk
Street Scene (Ramachandra and Jones)	2020	Se	1	203,257	56,847	146,410	17	Vehicle accidents, Illegal turns, Illegal occupations, Retrograde motion, Pedestrian on road, Road spills, The else
TAD (Lv et al)	2021	We	-	540,272	452,220	88,052	7	Running, Falling, Fighting, Sleeping, Crawling, Having a seizure, Laying down, Dancing, Stealing, Rotating 360 degrees, Shuffling, Walking injured, Walking drunk, Stumbling walk, People and car accident, Car crash, Running injured, Fire, Smoke, Jaywalking, Driving outside lane, Jumping
UBnormal (Acsintoae et al)	2022	Su	29	236,902	116,087	92,640	22	Climbing fence, Car crossing square, Cycling on footpath, Kicking trash can, Jaywalking, Snatching bag, Crossing lawn, Wrong turn, Cycling on square, Chasing, Loitering, Scuffle, Littering, Forgetting backpack, U-turn, Battering, Driving on wrong side, Falling, Suddenly stopping cycling in the middle of the road, Group conflict, Climbing tree, Stealing, Illegal parking, Trucks, Protest, Playing with water, Photographing in restricted area, Dogs
NWPU Campus (Cao et al)	2023	Se	43	1,466,073	1,082,014	384,059	28	

it cannot give enough information to evaluate attribute-based explainable methods.

Avenue (Ave) (Lu et al, 2013b)

offers a discerning collection of videos specifically curated for anomaly detection research. Constituting videos primarily focused on avenues, the dataset provides researchers with a variety of challenging scenarios under diverse environmental and lighting conditions. It uniquely encompasses a wide range of anomalous events, such as loitering, throwing objects, and running, amidst everyday pedestrian activities. Captured via fixed-position cameras, the dataset facilitates explainability evaluations by providing a balanced mixture of ordinary and anomalous events. Like Ped2, it only works for attention-based explainable methods.

Street Scene (SST) (Ramachandra and Jones, 2020)

has 46 training and 35 testing video sequences, all captured at a high resolution of 1280×720 ,

observing a bustling two-lane street scene during daytime hours. With an enriched tapestry of activities, including cars navigating, and pedestrians in varied motions, the dataset introduces multi-faceted challenges for anomaly detection. Remarkably, Street Scene contains 205 naturally occurring anomalous events, which span illegal activities such as jaywalking and unauthorized U-turns, infrequent occurrences like pet-walking and meter maid interventions, thereby serving as a comprehensive benchmark for developing and evaluating anomaly detection models in the complexity and variability of urban environments.

UCF-Crime (UCF) (Sultani et al, 2018)

represents a substantial contribution to the domain of anomaly detection, boasting 1,900 videos that encompass 13 distinct anomalous event categories, recorded via indoor and outdoor CCTV cameras under varied lighting conditions. Categories encompass a wide spectrum of unlawful and disruptive activities including,

but not limited to, Abuse, Arrest, Assaults, and Burglary, thereby providing a comprehensive and challenging framework for the development and empirical evaluation of video anomaly detection algorithms amidst a variety of complex, real-world scenarios. This provides a rich context for models to show their explainability. This dataset provides detailed anomaly labels useful in almost all existing explainable methods, including reasoning-based and attribute-based methods.

ShanghaiTech Campus (STC) (Zhang et al, 2016)

includes a varied compilation of 437 videos, with durations spanning 15 seconds to over a minute, recorded under an array of circumstances and illumination conditions in outdoor settings via CCTV cameras. Notably, it presents multifaceted challenges through its inclusion of complex lighting situations and multiple camera angles, thereby establishing a comprehensive platform for researchers to delve into, evaluate, and develop anomaly detection algorithms within contextually rich and diversely illuminated environments. This dataset provides detailed actions and complex anomalies, so some explainable techniques like scene graph can work well in this dataset, which is suitable for attention-based method and reasoning-based methods.

NWPU Campus (Cao et al, 2023a)

is proposed for semi-supervised video anomaly detection. It stands as the largest and most complex dataset in its field, encompassing 43 scenes, 28 classes of anomalous events, and a total of 16 hours of video footage. Notably, it includes scene-dependent anomalies, indicating that an event might be considered normal in one scene but abnormal in another. It is suitable for interpreting VAD models in complex scenarios. Consequently, this characteristic presents a challenging problem for developing scene-specific explainable methods.

XD-violence (XD) (Wu et al, 2020)

focuses on recognizing and understanding violent activities. This dataset is meticulously compiled, comprising a diverse array of videos that encapsulate various facets and degrees of violent actions in numerous settings and contexts. Encompassing scenarios that range from mild altercations

to more severe and explicit forms of violence, the XD-violence dataset poses a complex challenge for video anomaly detection models. It not only serves as a comprehensive benchmark for evaluating the efficacy of existing models but also catalyzes the advancement of novel methods tailored to discern and categorize different intensities and natures of violent activities amidst multifarious environmental variables. This dataset has comprehensive anomaly events and labels which make it suitable for most of the explainable methods.

X-MAN (Szymanowicz et al, 2021)

is derived and reannotated from notable datasets like ShanghaiTech, Avenue, and UCSD Ped2. Each frame is meticulously annotated with between 1 and 5 explanation labels, each elucidating a distinct rationale for the frame’s anomaly, thereby catering to a multitude of anomalous events within a singular frame—such as simultaneous occurrences of running and bike-riding. Cumulatively, the dataset gives 40,618 labels across all frames, with a predominant 22,640 anomalies attributed to actions, followed by 14,828 ascribed to anomalous objects, while the residual pertains to anomalies related to location. Significantly, the dataset delineates 42 anomalous actions and 13 anomalous objects, presenting a comprehensive, multi-faceted benchmark for developing and assessing anomaly detection algorithms in varied contexts. It is designed for evaluating explainable methods with detailed anomaly reasons, making it suitable for attribute-based methods.

UBnormal (Acsintoae et al, 2022)

is an open-set, supervised collection of various virtual scenes designed for video anomaly detection. It stands out from current datasets by providing pixel-level annotations of abnormal events during training, which allows for the employment of fully-supervised learning techniques in detecting unusual events for the first time. To preserve the open-set structure, the developers have carefully arranged for different types of anomalies to be present in the training and testing video sets. This dataset provides pixel-level anomaly labels, so it can be applied to evaluate explainability, such as localization, for the explainable VAD method.

TAD (Lv et al, 2021)

focuses on traffic anomalies, differing significantly from other anomaly detection benchmarks by covering real-world traffic conditions. It aims to enhance the diversity and complexity of anomaly detection scenarios, particularly in traffic monitoring for early warning and emergency assistance, by including various real-world anomalies across different conditions and times of day. Since existing anomaly detection methods primarily focus on human behavior, the traffic anomaly dataset bridges the gap for traffic anomaly detection scenarios. Furthermore, it provides object-level labels and annotations for anomalous events, which makes quantifying explainability possible.

6 Evaluation Metrics

6.1 For images

Image-level metrics

For image-level anomaly detection, i.e., determining whether the sample is anomalous or not, the most prominent metrics are the Area Under the Receiver Operating Characteristic (AUROC) and the Area Under the Precision-Recall curve (AUPR). The ROC curve is a visual plot that demonstrates the performance of a binary classification system across a range of decision thresholds. It maps the rate of true positives (TPR) to the rate of false positives (FPR) on a graph. The AUROC quantifies the overall ability of the classifier to distinguish between the positive and negative classes. An anomaly detector with an AUROC score of 0.5 suggests that the model is random guessing, whereas a score of 1 signifies an impeccable anomaly detector. Precision-recall curves are particularly beneficial for assessing classification in imbalanced datasets. The AUPR offers a summarized measure of the classifier’s performance across different thresholds. For datasets with a significantly low anomaly ratio, the AUPR can be more informative than the AUROC.

Pixel-level metrics

For pixel-level anomaly localization and segmentation of images, the most commonly adopted evaluation metrics are AUROC and IoU (Intersection over Union). Assessing the effectiveness of

anomaly segmentation techniques at the pixel-by-pixel scale considers the result of classifying each pixel to be of equal significance. Just as image-level anomaly detection, a pixel’s classification can also fall into one of four categories: TP, TN, FP, or FN. For each scenario, the aggregate count of pixels from the test dataset is determined as:

$$\text{TP} = \sum_{i=1}^n |\{p \mid L_i(p) = 1\} \cap \{p \mid S_i(p) > t\}|, \quad (9)$$

$$\text{TN} = \sum_{i=1}^n |\{p \mid L_i(p) = 0\} \cap \{p \mid S_i(p) \leq t\}|, \quad (10)$$

$$\text{FP} = \sum_{i=1}^n |\{p \mid L_i(p) = 0\} \cap \{p \mid S_i(p) > t\}|, \quad (11)$$

$$\text{FN} = \sum_{i=1}^n |\{p \mid L_i(p) = 1\} \cap \{p \mid S_i(p) \leq t\}|, \quad (12)$$

where p denotes each pixel, i denotes the i -th testing sample, S_i denotes the associated anomaly score at pixel p of sample i , and L_i denotes the pixel level ground truth label that can either be 0 or 1, signifying the absence or presence of an anomaly respectively. Here $|\cdot|$ denotes the cardinality of the inside set and t denotes the threshold for anomaly classification. Using these comprehensive measures, which are influenced by the total pixel count in the dataset, we can derive relative metrics like the per-pixel true positive rate (TPR), false positive rate (FPR), and precision (PRC) as in the image-level metrics section.

While several metrics exist for evaluating segmentation algorithms, the Intersection over Union (IoU) metric stands out for its efficacy. Specifically, within the realm of anomaly segmentation, the set of anomalous predictions is denoted as $P = \bigcup_{i=1}^n \{p \mid S_i(p) > t\}$, and the set of ground truth anomalous pixels is represented as $G = \bigcup_{i=1}^n \{p \mid L_i(p) = 1\}$. In parallel to the aforementioned relative metrics, the IoU for the ‘anomalous’ category can be articulated using absolute pixel classification metrics as:

$$\text{IoU} = \frac{|P \cap G|}{|P \cup G|} = \frac{\text{TP}}{\text{TP} + \text{FP} + \text{FN}}. \quad (13)$$

While these metrics are straightforward, their pixel-independent nature can bias results toward larger anomalous regions (Bergmann et al, 2019, 2021). Detecting one extensive defect might offset multiple undetected minor defects. Given the variance in defect sizes across the proposed dataset, it’s crucial to consider metrics based on each ground truth’s connected component, leading to Region-level metrics.

Region-level metrics

Rather than assessing each pixel individually, metrics at the region level take an average performance across each contiguous segment of the actual data. This method is particularly beneficial when recognizing tiny irregularities is deemed as crucial as spotting larger ones, a scenario commonly found in real-world applications. The most commonly used region-level metric in anomaly segmentation is the per-region overlap (PRO) metric. To start, each test image’s actual data is broken down into its connected segments. Suppose $A_{i,j}$ represents the group of pixels identified as anomalies for a particular segment j in the authentic image i , and G_i stands for the group of pixels anticipated to be anomalous at a set threshold t . The PRO can subsequently be calculated as

$$\text{PRO} = \frac{1}{N} \sum_i \sum_k \frac{|G_i \cap A_{i,j}|}{A_{i,j}}, \quad (14)$$

where N represents the total count of true elements in the dataset under evaluation. The PRO metric bears a strong resemblance to the TPR. The key distinction is that, with PRO, the TPR is averaged across each ground truth region rather than across every individual pixel in the image.

6.2 For videos

Besides the AUC that is used in both image video anomaly detection and video anomaly detection, there are some unique metrics for videos.

Track-Based Detection Rate (Ramachandra and Jones, 2020)

In the realm of video anomaly detection, where accurate identification and classification of anomalous activities are paramount, the Track-Based Detection Rate (TBDR) metric emerges as

a pivotal criterion, meticulously assessing detection performance across video sequences. The TBDR quantitatively juxtaposes the number of accurately detected anomalous tracks against the total number of anomalous tracks present, as expressed in

$$\text{TBDR} = \frac{\text{num. of anomalous tracks detected}}{\text{total num. of anomalous tracks}} \quad (15)$$

An anomalous track is deemed detected if at least a fraction α of the ground truth regions within the track is identified, and a ground truth region in a frame is considered detected if the Intersection Over Union (IOU) with a detected region is at least β . Concurrently, the False Positive Rate per frame (FPR), expressed as

$$\text{FPR} = \frac{\text{total false positive regions}}{\text{total frames}} \quad (16)$$

It underscores the model’s precision by quantifying the number of falsely identified regions relative to total frames, whereby a detected region is labeled as a false positive if the IOU with every ground truth region in the frame is $< \beta$. Significantly, while a singular detected region might encompass two or more ground truth regions, ensuring each truth region is detected, such occurrences are sporadic, thereby entrenching TBDR as a vital metric in distilling the efficacy and precision of anomaly detection models within complex video datasets.

RBDR: Region-Based Detection Criterion (Ramachandra and Jones, 2020)

The RBDR is determined across all frames in a test set in relation to the quantity of false positive regions for each frame, which can be mathematically expressed as

$$\text{RBDR} = \frac{\text{num. of anomalous regions detected}}{\text{total num. of anomalous regions}} \quad (17)$$

It assesses detection capabilities by appraising the number of precisely detected anomalous regions about the entirety of anomalous regions present. Similar to the track-based criterion, a region of ground truth is considered successfully detected if the overlap measure, known as the Intersection Over Union (IOU), between the actual ground

truth and the detected region is at least β . The RBDR considers all ground truth anomalous regions throughout the entirety of frames within a test set. Simultaneously, the number of false positives per frame is evaluated similarly to the track-based detection criterion. Embarking on detection criteria inevitably lands on the balance between detection rate (true positive rate) and false positive rate, a relationship which can be elucidated through a Receiver Operating Characteristic (ROC) curve, deduced by varying the threshold on the anomaly score dictating the detection of anomalous regions. When a singular evaluative figure is sought, the performance is adeptly summarized utilizing the average detection rate for false positive rates ranging from 0 to 1, i.e., the area under the ROC curve for false positive rates ≤ 1 .

7 Future Directions

7.1 Quantifying explainable methods

In the VAD task, there are plenty of explainable methods that give explanations from every aspect, including pixel level, object level, and so on. However, none of them has quantified their explanation performance. [Szymanowicz et al \(2021\)](#) tried to quantify the explanation performance by showing the anomaly classification performance, but other methods can barely follow due to the different explanation directions. In this case, rather than showing some selected examples to prove the effectiveness of one method, it is better to quantify the effectiveness of an explainable method. For example, if a method explains by providing an attention map to illustrate the explanation, it is preferred to use the Intersection Over Union metric like the image segmentation task. A dataset with such ground truths is also needed to achieve the target. In addition, existing metrics in explainable AI can be adapted for anomaly explanation, including those using feature importance (e.g., Saliency ([Simonyan et al, 2013](#)), Gradient SHAP ([Lundberg and Lee, 2017](#)), Deepflit ([Shrikumar et al, 2017](#)), Representation Latent Shift ([Crabbé and van der Schaar, 2022](#)), etc.) and Example Importance (e.g., Influence

Function ([Koh and Liang, 2017](#)), Tracing Gradient Descent ([Pruthi et al, 2020](#)), Importance Score ([Crabbé and van der Schaar, 2022](#)), etc.).

7.2 Explaining the anomaly detection methods involving self-supervised learning

Current state-of-the-art 2D anomaly detection methods, either for the image or video data, are more or less related to self-supervised learning ([Tack et al, 2020](#); [Georgescu et al, 2021a](#); [Wang et al, 2022c](#)). However, there exist few works clearly explaining why creating pretext tasks can improve anomaly detection performance. The main difficulty in interpreting the self-supervised anomaly detection techniques lies in that it is hard to explain the performance difference between the normal and abnormal samples on the auxiliary task. To investigate the explainability of such methods, researchers may need to refer to the theory of self-supervision and data augmentation.

7.3 Building new benchmarks for explainable 2D anomaly detection

Existing image and video anomaly detection benchmarks ([Bergmann et al, 2019](#); [Mahadevan et al, 2010a](#); [Lu et al, 2013a](#); [Liu et al, 2018](#)) are still too simple and ideal for real-world applications. One unavoidable and important issue is that normal objects or behaviors in one background might be normal in another. For instance, two people punching each other is considered normal in the boxing ring, while abnormal in the classroom. Therefore, new benchmarks are needed for deceptive cases, and desired methods should conduct reasoning among background and objects with sensible explanations.

7.4 Foundation models for 2D anomaly detection

Foundation models or large pre-trained models, such as GPT-4 ([Achiam et al, 2023](#)), LLaVA ([Liu et al, 2023a](#)), SAM ([Kirillov et al, 2023](#)), and DINO ([Liu et al, 2023b](#)), have demonstrated exceptional capabilities in reasoning and understanding images. These models are particularly powerful due to their pre-training on vast datasets

comprising images and their associated textual descriptions. Consequently, they possess the ability to discern normal and abnormal objects when presented with either images or text. This intrinsic knowledge proves invaluable for various downstream tasks, including image anomaly detection and video anomaly detection. For instance, AnomalyGPT (Gu et al, 2023) leveraged the large multi-modal model, pandaGPT (Su et al, 2023), to detect anomalies in images. By simply inputting an image to pandaGPT and asking whether anomalies are present, their method not only identifies anomalies but also provides explanations, such as identifying cracks or cuts. On the other hand, SAA (Cao et al, 2023b) localizes anomalies without the need for explicit training. They achieve this by adapting existing foundation models, DINO (Liu et al, 2023b) and SAM (Kirillov et al, 2023), through hybrid prompt regularization. These successful applications of foundation models in image anomaly detection underscore their robust anomaly detection capabilities. However, current methods harness only a fraction of the potential offered by foundation models, such as their zero-shot and few-shot abilities. The extensive reasoning capabilities of these models remain largely unexplored. Notably, there has been a lack of research applying foundation models to video anomaly detection, primarily due to the complexity of video anomalies. In video anomaly detection, anomalies encompass multiple dimensions, including object anomalies, motion anomalies, and even background anomalies. Simple retrieval methods are often insufficient for this task. However, with the aid of their advanced reasoning abilities, foundation models can easily discern whether a particular motion is plausible within a given background context and provide explanations. Moreover, foundation models offer a promising approach for adapting to various scenes. For instance, while street fighting should be classified as an anomaly, it is normal within an octagonal cage context. Traditional video anomaly detection models struggle to distinguish between these scenarios, often leading to incorrect predictions. In contrast, foundation models can effectively handle such distinctions with their extensive parameterization, enabling them to treat different scenes separately.

8 Conclusion

This paper presents the first survey on explainable anomaly detection for 2D visual data. The explainable and interpretable anomaly detection approaches for both images and videos are thoroughly summarized and how these methods explain the anomaly identification process is well elaborated. The reasons why certain explainable anomaly detection methods are applicable to both images and videos, while others are limited to a single modality are further explored. Moreover, summaries of current datasets and evaluation metrics for 2D visual anomaly detection are offered. The survey is closed by pointing out some future directions for a deeper and better understanding of anomaly detection in images and videos.

Data Availability

Data or code from this study are available from the corresponding author upon reasonable request.

References

- Abati D, Porrello A, Calderara S, et al (2019) Latent space autoregression for novelty detection. In: CVPR
- Achiam J, Adler S, Agarwal S, et al (2023) Gpt-4 technical report. arXiv preprint arXiv:230308774
- Acsintoae A, Florescu A, Georgescu MI, et al (2022) Ubnormal: New benchmark for supervised open-set video anomaly detection. In: Proceedings of the IEEE/CVF Conference on Computer Vision and Pattern Recognition, pp 20143–20153
- Adadi A, Berrada M (2018) Peeking inside the black-box: a survey on explainable artificial intelligence (xai). IEEE access
- Adam A, Rivlin E, Shimshoni I, et al (2008) Robust real-time unusual event detection using multiple fixed-location monitors. IEEE transactions on pattern analysis and machine intelligence 30(3):555–560
- Bergmann P, Fauser M, Sattlegger D, et al (2019) Mvtec ad—a comprehensive real-world dataset for unsupervised anomaly detection. In: CVPR

- Bergmann P, Fauser M, Sattlegger D, et al (2020) Uninformed students: Student-teacher anomaly detection with discriminative latent embeddings. In: CVPR
- Bergmann P, Batzner K, Fauser M, et al (2021) The mvtec anomaly detection dataset: a comprehensive real-world dataset for unsupervised anomaly detection. *International Journal of Computer Vision* 129(4):1038–1059
- Bergmann P, Batzner K, Fauser M, et al (2022) Beyond dents and scratches: Logical constraints in unsupervised anomaly detection and localization. *International Journal of Computer Vision* 130(4):947–969
- Blum H, Sarlin PE, Nieto J, et al (2019) Fishyscapes: A benchmark for safe semantic segmentation in autonomous driving. In: proceedings of the IEEE/CVF international conference on computer vision workshops, pp 0–0
- Božić J, Tabernik D, Skočaj D (2021) Mixed supervision for surface-defect detection: From weakly to fully supervised learning. *Computers in Industry* 129:103459
- Cao C, Lu Y, Wang P, et al (2023a) A new comprehensive benchmark for semi-supervised video anomaly detection and anticipation. In: Proceedings of the IEEE/CVF Conference on Computer Vision and Pattern Recognition, pp 20392–20401
- Cao Y, Xu X, Sun C, et al (2023b) Segment any anomaly without training via hybrid prompt regularization. arXiv preprint arXiv:230510724
- Cao Y, Xu X, Sun C, et al (2023c) Towards generic anomaly detection and understanding: Large-scale visual-linguistic model (gpt-4v) takes the lead. arXiv preprint arXiv:231102782
- Cao Y, Xu X, Zhang J, et al (2024) A survey on visual anomaly detection: Challenge, approach, and prospect. arXiv preprint arXiv:240116402
- Cao YH, Wu J (2022) A random cnn sees objects: One inductive bias of cnn and its applications. In: AAAI
- Chan R, Lis K, Uhlemeyer S, et al (2021) Segmentmeifyoucan: A benchmark for anomaly segmentation. arXiv preprint arXiv:210414812
- Chen C, Xie Y, Lin S, et al (2022) Comprehensive regularization in a bi-directional predictive network for video anomaly detection. In: AAAI
- Chen N, Du Z, Ng KH (2018) Scene graphs for interpretable video anomaly classification. In: NeurIPS Workshop on Visually Grounded Interaction and Language
- Chen X, Zhang J, Tian G, et al (2023) Clipad: A language-guided staged dual-path model for zero-shot anomaly detection. arXiv preprint arXiv:231100453
- Cohen MJ, Avidan S (2022) Transformally-two (feature spaces) are better than one. In: CVPR
- Cordts M, Omran M, Ramos S, et al (2016) The cityscapes dataset for semantic urban scene understanding. In: Proceedings of the IEEE conference on computer vision and pattern recognition, pp 3213–3223
- Crabbé J, van der Schaar M (2022) Label-free explainability for unsupervised models. arXiv preprint arXiv:220301928
- Doshi K, Yilmaz Y (2023) Towards interpretable video anomaly detection. In: WACV
- Fei-Fei L, Fergus R, Perona P (2004) Learning generative visual models from few training examples: An incremental bayesian approach tested on 101 object categories. In: 2004 conference on computer vision and pattern recognition workshop, IEEE, pp 178–178
- Georgescu MI, Barbalau A, Ionescu RT, et al (2021a) Anomaly detection in video via self-supervised and multi-task learning. In: CVPR
- Georgescu MI, Ionescu RT, Khan FS, et al (2021b) A background-agnostic framework with adversarial training for abnormal event detection in video. *IEEE TPAMI*
- Gong D, Liu L, Le V, et al (2019) Memorizing normality to detect anomaly: Memory-augmented

- deep autoencoder for unsupervised anomaly detection. In: CVPR
- Gu Z, Zhu B, Zhu G, et al (2023) Anomalygpt: Detecting industrial anomalies using large vision-language models. arXiv preprint arXiv:230815366
- Gudovskiy D, Ishizaka S, Kozuka K (2022) Cflowad: Real-time unsupervised anomaly detection with localization via conditional normalizing flows. In: Proceedings of the IEEE/CVF Winter Conference on Applications of Computer Vision, pp 98–107
- Hasan M, Choi J, Neumann J, et al (2016) Learning temporal regularity in video sequences. In: CVPR
- He H, Zhang J, Chen H, et al (2023) Diad: A diffusion-based framework for multi-class anomaly detection. arXiv preprint arXiv:231206607
- Hinami R, Mei T, Satoh S (2017) Joint detection and recounting of abnormal events by learning deep generic knowledge. In: ICCV
- Ho J, Jain A, Abbeel P (2020) Denoising diffusion probabilistic models. NeurIPS
- Hochreiter S, Schmidhuber J (1997) Long short-term memory. *Neural computation*
- Hsu YC, Shen Y, Jin H, et al (2020) Generalized odin: Detecting out-of-distribution image without learning from out-of-distribution data. In: CVPR
- Huang Y, Qiu C, Yuan K (2020) Surface defect saliency of magnetic tile. *The Visual Computer* 36:85–96
- Irvin J, Rajpurkar P, Ko M, et al (2019) Chexpert: A large chest radiograph dataset with uncertainty labels and expert comparison. In: Proceedings of the AAAI conference on artificial intelligence, pp 590–597
- Jeong J, Zou Y, Kim T, et al (2023) Winclip: Zero-/few-shot anomaly classification and segmentation. In: Proceedings of the IEEE/CVF Conference on Computer Vision and Pattern Recognition, pp 19606–19616
- Jezek S, Jonak M, Burget R, et al (2021) Deep learning-based defect detection of metal parts: evaluating current methods in complex conditions. In: 2021 13th International congress on ultra modern telecommunications and control systems and workshops (ICUMT), IEEE, pp 66–71
- Jiang X, Xie G, Wang J, et al (2022) A survey of visual sensory anomaly detection. arXiv preprint arXiv:220207006
- Khan SS, Madden MG (2010) A survey of recent trends in one class classification. In: Artificial Intelligence and Cognitive Science: 20th Irish Conference, AICS 2009, Dublin, Ireland, August 19-21, 2009, Revised Selected Papers 20, Springer, pp 188–197
- Kirillov A, Mintun E, Ravi N, et al (2023) Segment anything. arXiv:230402643
- Koh PW, Liang P (2017) Understanding black-box predictions via influence functions. In: International conference on machine learning, PMLR, pp 1885–1894
- Krizhevsky A, Hinton G, et al (2009) Learning multiple layers of features from tiny images. Master’s thesis, Department of Computer Science, University of Toronto
- Kuijff HJ, Biesbroek JM, De Bresser J, et al (2019) Standardized assessment of automatic segmentation of white matter hyperintensities and results of the wmh segmentation challenge. *IEEE transactions on medical imaging* 38(11):2556–2568
- Kwon G, Prabhushankar M, Temel D, et al (2020) Backpropagated gradient representations for anomaly detection. In: ECCV
- Kylberg G (2011) Kylberg texture dataset v. 1.0. Centre for Image Analysis, Swedish University of Agricultural Sciences and . . .
- Langone R, Cuzzocrea A, Skantzos N (2020) Interpretable anomaly prediction: Predicting

- anomalous behavior in industry 4.0 settings via regularized logistic regression tools. *Data & Knowledge Engineering*
- LeCun Y, Bottou L, Bengio Y, et al (1998) Gradient-based learning applied to document recognition. *Proceedings of the IEEE* 86(11):2278–2324
- Lee K, Lee K, Lee H, et al (2018) A simple unified framework for detecting out-of-distribution samples and adversarial attacks. *NeurIPS*
- Lesjak Ž, Galimzianova A, Koren A, et al (2018) A novel public mr image dataset of multiple sclerosis patients with lesion segmentations based on multi-rater consensus. *Neuroinformatics* 16:51–63
- Li L, Xu M, Wang X, et al (2019) Attention based glaucoma detection: A large-scale database and cnn model. In: *Proceedings of the IEEE/CVF conference on computer vision and pattern recognition*, pp 10571–10580
- Li S, Cao J, Ye P, et al (2024) Clipsam: Clip and sam collaboration for zero-shot anomaly segmentation. *arXiv preprint arXiv:240112665*
- Li Y, Wang H, Yuan S, et al (2023a) Myriad: Large multimodal model by applying vision experts for industrial anomaly detection. *arXiv preprint arXiv:231019070*
- Li Z, Zhu Y, Van Leeuwen M (2023b) A survey on explainable anomaly detection. *ACM Trans Knowl Discov Data* 18(1). <https://doi.org/10.1145/3609333>, URL <https://doi.org/10.1145/3609333>
- Liang S, Li Y, Srikant R (2018) Enhancing the reliability of out-of-distribution image detection in neural networks. In: *ICLR*
- Liu H, Li C, Wu Q, et al (2023a) Visual instruction tuning
- Liu S, Zeng Z, Ren T, et al (2023b) Grounding dino: Marrying dino with grounded pre-training for open-set object detection
- Liu W, Luo W, Lian D, et al (2018) Future frame prediction for anomaly detection—a new baseline. In: *CVPR*
- Liu W, Li R, Zheng M, et al (2020) Towards visually explaining variational autoencoders. In: *CVPR*
- Liu Z, Luo P, Wang X, et al (2015) Deep learning face attributes in the wild. In: *Proceedings of the IEEE international conference on computer vision*, pp 3730–3738
- Liu Z, Nie Y, Long C, et al (2021) A hybrid video anomaly detection framework via memory-augmented flow reconstruction and flow-guided frame prediction. In: *ICCV*
- Liznerski P, Ruff L, Vandermeulen RA, et al (2021) Explainable deep one-class classification. In: *ICLR*
- Lu C, Shi J, Jia J (2013a) Abnormal event detection at 150 fps in matlab. In: *ICCV*
- Lu C, Shi J, Jia J (2013b) Abnormal event detection at 150 fps in matlab. In: *Proceedings of the IEEE international conference on computer vision*, pp 2720–2727
- Lundberg SM, Lee SI (2017) A unified approach to interpreting model predictions. *Advances in neural information processing systems* 30
- Luo W, Liu W, Gao S (2017) Remembering history with convolutional lstm for anomaly detection. In: *ICME*
- Lv H, Sun Q (2024) Video anomaly detection and explanation via large language models. *arXiv preprint arXiv:240105702*
- Lv H, Zhou C, Cui Z, et al (2021) Localizing anomalies from weakly-labeled videos. *IEEE transactions on image processing* 30:4505–4515
- Maaz M, Rasheed H, Khan S, et al (2023) Videochatgpt: Towards detailed video understanding via large vision and language models. *arXiv preprint arXiv:230605424*
- Mahadevan V, Li W, Bhalodia V, et al (2010a) Anomaly detection in crowded scenes. In:

CVPR

- Mahadevan V, Li W, Bhalodia V, et al (2010b) Anomaly detection in crowded scenes. In: 2010 IEEE Computer Society Conference on Computer Vision and Pattern Recognition, pp 1975–1981, <https://doi.org/10.1109/CVPR.2010.5539872>
- Menze BH, Jakab A, Bauer S, et al (2014) The multimodal brain tumor image segmentation benchmark (brats). *IEEE transactions on medical imaging* 34(10):1993–2024
- Mishra P, Verk R, Fornasier D, et al (2021) Vt-adl: A vision transformer network for image anomaly detection and localization. In: 2021 IEEE 30th International Symposium on Industrial Electronics (ISIE), IEEE, pp 01–06
- Mohammadi B, Fathy M, Sabokrou M (2021) Image/video deep anomaly detection: A survey. arXiv preprint arXiv:210301739
- Nesen A, Bhargava B (2020) Knowledge graphs for semantic-aware anomaly detection in video. In: AIKE
- Netzer Y, Wang T, Coates A, et al (2011) Reading digits in natural images with unsupervised feature learning. In: NIPS workshop on deep learning and unsupervised feature learning, Granada, Spain, p 7
- Pang G, Yan C, Shen C, et al (2020) Self-trained deep ordinal regression for end-to-end video anomaly detection. In: CVPR
- Pang G, Ding C, Shen C, et al (2021) Explainable deep few-shot anomaly detection with deviation networks. arXiv preprint arXiv:210800462
- Perera P, Nallapati R, Xiang B (2019) Ocgan: One-class novelty detection using gans with constrained latent representations. In: Proceedings of the IEEE/CVF conference on computer vision and pattern recognition, pp 2898–2906
- Perera P, Oza P, Patel VM (2021) One-class classification: A survey. arXiv preprint arXiv:210103064
- Pinaya WH, Graham MS, Gray R, et al (2022) Fast unsupervised brain anomaly detection and segmentation with diffusion models. In: MICCAI
- Pruthi G, Liu F, Kale S, et al (2020) Estimating training data influence by tracing gradient descent. *Advances in Neural Information Processing Systems* 33:19920–19930
- Purwanto D, Chen YT, Fang WH (2021) Dance with self-attention: A new look of conditional random fields on anomaly detection in videos. In: ICCV
- Radford A, Kim JW, Hallacy C, et al (2021) Learning transferable visual models from natural language supervision. In: International conference on machine learning, PMLR, pp 8748–8763
- Raghavendra R, Bue A, Cristani M (2006) Unusual crowd activity dataset of university of minnesota
- Ramachandra B, Jones M (2020) Street scene: A new dataset and evaluation protocol for video anomaly detection. In: Proceedings of the IEEE/CVF Winter Conference on Applications of Computer Vision, pp 2569–2578
- Ramachandra B, Jones MJ, Vatsavai RR (2020) A survey of single-scene video anomaly detection. *IEEE TPAMI*
- Reiss T, Hoshen Y (2022) Attribute-based representations for accurate and interpretable video anomaly detection. arXiv preprint arXiv:221200789
- Reiss T, Cohen N, Bergman L, et al (2021) Panda: Adapting pretrained features for anomaly detection and segmentation. In: CVPR
- Ren J, Liu PJ, Fertig E, et al (2019) Likelihood ratios for out-of-distribution detection. *NeurIPS*
- Ristea NC, Madan N, Ionescu RT, et al (2022) Self-supervised predictive convolutional attentive block for anomaly detection. In: CVPR

- Ronneberger O, Fischer P, Brox T (2015) U-net: Convolutional networks for biomedical image segmentation. In: MICCAI
- Roth K, Pemula L, Zepeda J, et al (2022) Towards total recall in industrial anomaly detection. In: CVPR
- Salehi M, Sadjadi N, Baselizadeh S, et al (2021) Multiresolution knowledge distillation for anomaly detection. In: CVPR
- Schlegl T, Seeböck P, Waldstein SM, et al (2017) Unsupervised anomaly detection with generative adversarial networks to guide marker discovery. In: IPMI
- Schlegl T, Seeböck P, Waldstein SM, et al (2019) f-anogan: Fast unsupervised anomaly detection with generative adversarial networks. Medical image analysis
- Selvaraju RR, Cogswell M, Das A, et al (2017) Grad-cam: Visual explanations from deep networks via gradient-based localization. In: ICCV
- Shrikumar A, Greenside P, Kundaje A (2017) Learning important features through propagating activation differences. In: International conference on machine learning, PMLR, pp 3145–3153
- Simonyan K, Vedaldi A, Zisserman A (2013) Deep inside convolutional networks: Visualising image classification models and saliency maps. arXiv preprint arXiv:13126034
- Singh A, Jones MJ, Learned-Miller E (2022) Eval: Explainable video anomaly localization. arXiv preprint arXiv:221207900
- Su Y, Lan T, Li H, et al (2023) Pandagpt: One model to instruction-follow them all. arXiv preprint arXiv:230516355
- Sudlow C, Gallacher J, Allen N, et al (2015) Uk biobank: an open access resource for identifying the causes of a wide range of complex diseases of middle and old age. PLoS medicine 12(3):e1001779
- Sultani W, Chen C, Shah M (2018) Real-world anomaly detection in surveillance videos. In: Proceedings of the IEEE conference on computer vision and pattern recognition, pp 6479–6488
- Szymanowicz S, Charles J, Cipolla R (2021) X-man: Explaining multiple sources of anomalies in video. In: CVPR
- Szymanowicz S, Charles J, Cipolla R (2022) Discrete neural representations for explainable anomaly detection. In: WACV
- Tabernik D, Šela S, Skvarč J, et al (2020) Segmentation-based deep-learning approach for surface-defect detection. Journal of Intelligent Manufacturing 31(3):759–776
- Tack J, Mo S, Jeong J, et al (2020) Csi: Novelty detection via contrastive learning on distributionally shifted instances. NeurIPS
- Tang Y, Zhao L, Zhang S, et al (2020) Integrating prediction and reconstruction for anomaly detection. Pattern Recognition Letters
- Temel D, Kwon G, Prabhushankar M, et al (2017) Cure-tsr: Challenging unreal and real environments for traffic sign recognition. arXiv preprint arXiv:171202463
- Venkataramanan S, Peng KC, Singh RV, et al (2020) Attention guided anomaly localization in images. In: ECCV
- Wang G, Wang Y, Qin J, et al (2022a) Video anomaly detection by solving decoupled spatio-temporal jigsaw puzzles. In: ECCV
- Wang Y, Qin C, Bai Y, et al (2022b) Making reconstruction-based method great again for video anomaly detection. In: ICDM
- Wang Y, Qin C, Wei R, et al (2022c) Self-supervision meets adversarial perturbation: A novel framework for anomaly detection. In: CIKM
- Wang Y, Zhang R, Wang H, et al (2023) Vaquita: Enhancing alignment in llm-assisted video understanding. arXiv preprint arXiv:231202310

- Wieler M, Hahn T (2007) Weakly supervised learning for industrial optical inspection. In: DAGM symposium in
- Wolleb J, Bieder F, Sandkühler R, et al (2022) Diffusion models for medical anomaly detection. In: MICCAI
- Wu P, Liu J (2021) Learning causal temporal relation and feature discrimination for anomaly detection. *IEEE TIP*
- Wu P, Liu J, Shi Y, et al (2020) Not only look, but also listen: Learning multimodal violence detection under weak supervision. In: *Computer Vision–ECCV 2020: 16th European Conference, Glasgow, UK, August 23–28, 2020, Proceedings, Part XXX 16*, Springer, pp 322–339
- Wyatt J, Leach A, Schmon SM, et al (2022) Anodpm: Anomaly detection with denoising diffusion probabilistic models using simplex noise. In: *CVPR Workshop*
- Xiao H, Rasul K, Vollgraf R (2017) Fashion-mnist: a novel image dataset for benchmarking machine learning algorithms. *arXiv preprint arXiv:170807747*
- Xiao Z, Yan Q, Amit Y (2020) Likelihood regret: An out-of-distribution detection score for variational auto-encoder. *NeurIPS*
- Xu P, Ehinger KA, Zhang Y, et al (2015) Turkergaze: Crowdsourcing saliency with webcam based eye tracking. *arXiv preprint arXiv:150406755*
- Yang J, Shi R, Ni B (2021a) Medmnist classification decathlon: A lightweight automl benchmark for medical image analysis. In: *IEEE 18th International Symposium on Biomedical Imaging (ISBI)*, pp 191–195
- Yang J, Zhou K, Li Y, et al (2021b) Generalized out-of-distribution detection: A survey. *arXiv preprint arXiv:211011334*
- Yang Z, Li L, Lin K, et al (2023) The dawn of llms: Preliminary explorations with gpt-4v (ision). *arXiv preprint arXiv:230917421* 9(1):1
- Yu F, Seff A, Zhang Y, et al (2015) Lsun: Construction of a large-scale image dataset using deep learning with humans in the loop. *arXiv preprint arXiv:150603365*
- Yu G, Wang S, Cai Z, et al (2020) Cloze test helps: Effective video anomaly detection via learning to complete video events. In: *ACM MM*, pp 583–591
- Yu J, Zheng Y, Wang X, et al (2021) Fastflow: Unsupervised anomaly detection and localization via 2d normalizing flows. *arXiv preprint arXiv:211107677*
- Zenati H, Romain M, Foo CS, et al (2018) Adversarially learned anomaly detection. In: *2018 IEEE International conference on data mining (ICDM)*, IEEE, pp 727–736
- Zhang J, Chen X, Xue Z, et al (2023) Exploring grounding potential of vqa-oriented gpt-4v for zero-shot anomaly detection. *arXiv preprint arXiv:231102612*
- Zhang Y, Zhou D, Chen S, et al (2016) Single-image crowd counting via multi-column convolutional neural network. In: *Proceedings of the IEEE conference on computer vision and pattern recognition*, pp 589–597
- Zhou B, Khosla A, Lapedriza A, et al (2016) Learning deep features for discriminative localization. In: *CVPR*
- Zhou Q, Pang G, Tian Y, et al (2023) Anomalyclip: Object-agnostic prompt learning for zero-shot anomaly detection. *arXiv preprint arXiv:231018961*
- Zou Y, Jeong J, Pemula L, et al (2022) Spot-the-difference self-supervised pre-training for anomaly detection and segmentation. In: *European Conference on Computer Vision*, Springer, pp 392–408